Thesis for the Degree of
Doctor of Philosophy

A Study on Improving Tool Life of Automotive Axle using Direct Metal Deposition Technology

Supervisor Prof. Jong Rae Cho

August 2018

Department of Mechanical Engineering
Korea Maritime and Ocean University

Shi Hai Chuan

본 논문을 HaiChuan Shi의 공학박사

학위논문으로 인준함.

위원장 손 동 우 (인)

위 원 조 종 래 (인)

위 원 심 도 식 (인)

위 원 고 정 혁 (인)

위 원 박 권 하 (인)

2018년 06월 29일

한국해양대학교 대학원

Contents

A study on improving tool life of automotive axle using direct metal deposition technology

Shi Hai Chuan

Department of Mechanical Engineering
Graduate School of Korea Maritime and Ocean University

Abstract

The working condition of hot forging die is very terrible, such as high temperature, high load, repeated thermal and loads. The life of hot forging die is generally lower than cold forging die, the cost of the workpieces and the economic efficiency of the manufactory are affected directly. Expecially for developing counties, average life of hot forging die is far lower than developed countries. It is essential to enhance the service life of hot forging die and to reduce cost of the pieces for hot forging industry.

The hot forging die simultaneously withstands the repetitive thermal load and the mechanical load, which can cause thermal stress and mechanical stress respectively. The thermal load is the main reason to cause damage of hot forging die. It is of great social and economic significance to study the surface hardening of tools and reduce the thermal stress precess.

This dissertation focuses on the early failure of the hot forging die for automotive axles, mainly by increasing the high-temperature strength of die to prevent thermal softening of tool surface. The surface hardening technology used in this study is direct metal deposition technology to deposit a high-performance metal on the surface of the traditional die that is easy for wear. However, thermal cracks are frequently generated on the deposited areas due to thermal stress from different material properties. A thermal stress control layer (TSCL) is designed to reduce thermal stress and increase fatigue life as a buffer in the vicinity of the joining region between the hardfacing layer and the base metal. TSCL and hardfacing layer are deposited through layer-by-layer way on the substrate using direct metal deposition technology. The TSCL to be produced by mixing of Stellite21 and SKD61 is designed with thicknesses of 0 mm, 1 mm, 1.5 mm, and 2 mm separately. The effect of thermal stress in the transition regions is investigated after adding TSCL. The optimal design of TSCL is selected by the change of thickness and composition proportion.

Stellite21 superalloy deposited on the hot forging die must undergo effects of repetitive thermal stress and mechanical stress during forging process. The hardening mechanism of Stellite21 is studied by microhardness tester. The etched Stellite21 samples are observed under the optical microscope. The microstructure analyses of Stellite21 are carried out on a TESCAN MIRA3 scanning electron microscope (SEM) with energy dispersive X-ray (EDX) spectrum. The phases present in the specimens are examined with an X-ray technique, using Cu K_radiation. So that the evolution microstructure and properties of Stellite21 are explained through before and after forging.

KEY WORDS: Hot forging die; Direct metal deposition technology; Thermal stress control layer; Stellite21 superalloy; Tool life.

List of Tables

List of Figures

Chapter 1 Introduction

1.1 Literature review

Forging technology in manufacturing field has a very important position because it helps to produce outstanding parts for mechanical properties with less waste of material.

In forging process, steel billet has a relatively simple geometry; this steel billet is plastically deformed into a product of relatively complex configuration after one or more operations. The service life of dies is very important due to cost reduction and finishing quality of productions. Especially for hot forging process, the extreme operation conditions of the hot working process often leads to premature failure of dies. In general, there are four types of failures for hot forging tools, such as thermal crack, mechanical fatigue, plastic deformation, and wear. Among these, wear is the dominant failure cause in hot forging dies[1,2]. Because the service life of dies are directly affects the cost of forgings and the economic benefit of production units. In the developed countries, tooling costs account for about 15% of the cost of forgings, while in the developing countries the costs account for more than 30%[3]. It is essential to enhance the service life of hot forging die and to reduce cost of the pieces for hot forging industry.

L. Cser et al. reported that wear was the dominating failure mechanism for forging dies, being accounted for approximately 70% of failures[2]. Several research papers describes that the wear of hot working tools is induced by thermal softening, as well as local bonding between the die and the workpiece[1,2,4-6]. To avoid surface damage in sliding process, shear stress must be restricted at the interface among the mating materials. The most commonly used solution is to add a lubricant to the forging system. This

method can reduce the shear stress, since it has the lowest shear resistance in forging process. As a consequence, the shear stress to affect the materials is significantly reduced, the friction is reduced and surface damage is avoided.

However, for some reasons, such as high temperature and complex shapes, lubrication may be partially failed, or it may not even be allowed for the forging system. The thermal softening of die surface can be prevent by increasing the high temperature strength of the hot forging die. The local deposition technology using laser is adopted to apply high strength materials. This deposition technology is very flexible and efficient for producing desired structures on hot forging dies, and it allows for mixing different powders while injecting them into the deposition region with the desired mixing ratio to create a special function region[7–9]. The local deposition technology can effectively improve the die life and reduce the manufacturing costs; however, thermal stress problems between the deposited layer and the base metal appear simultaneously. Some researchers have reported that thermal cracks are created in the vicinity of the intersection line between the deposited layer and the substrate[10,11].

In order to control thermal crack formation, advanced deposited technologies with multiple layers have been applied. Sörn Ocylok et al. had proposed using a functionally graded multi-layer approach as a buffer in the interface region [12]. Park et al. attempted to relieve the thermal stress by creating a thermal stress control layer (TSCL)[13]. The composition of TSCL is generally consist of the deposited material and the substrate. The optimal mixing ratio and thickness of TSCL is estimated via numerical analyses and experiments. Ahn et al. adopted a multi-type transition layer between the deposited region and the substrate to reduce mechanical and thermal issues, the results shown that a transition layer could dramatically improve the wear resistance of hot forging dies[14].

In addition, the appearance of the finite element method not only promoted the rapid development of engineering technology in the field of mechanics, but also solved major technical problems in many other fields[3]. In particular, the combination of finite element method and computer forms the basis of modern digital manufacturing. This also makes it to be possible to use the finite element software to simulate and analyze the failure causes of hot forging dies. The DEFORM software are useful for simulating the flow of 3D materials, also it is robust and easy to use. DEFORM powerful simulation engine can analyze the large deformation thermal properties of multiple associated objects in the metal forming process. The system integrates any necessary automatic triggering of the automatic grid repartition generator to generate an optimized grid system. In the areas with higher precision requirements, the fine grids can be divided to reduce the scale of operations and significantly increase computational efficiency. In this study, 2D-DEFORM software is used to analyze the wear and thermal stress of the hot forging die of automobile axle.

1.2 Thesis objectives

In this thesis, the service life of the axle hot forging die is researched, the wear region of the die is predicted using the finite element method. Serious wear region is determined by the surface pressure, surface temperature and the slipping velocity. A finite element model with a hardened layer is designed, Stellite21 superalloy is selected as the hardened layer material, since it can keep a well hardness at high temperature. SKD61 as a common tool steel is used to the substrate material of hot forging die. Due to the physical property difference between the Stellite21 and SKD61, large thermal stresses between the Stellite21 and SKD61 will be generated during hot forging process, it will be known clearly from finite element simulation results.

Thermal stress control layer (TSCL) is researched. It is designed the various TSCL to reduce the thermal stress between the Stellite21 and SKD61, TSCL with different thickness and composition proportion plays a different role in reducing thermal stress. The optimal thickness and ratio of TSCL is obtained from the simulation results. Finally, the hardened layer material after forging process is studied. After the repeated mechanical stress and thermal stress, the change of the microstructure and properties of the Stellite21 after forging are investigated.

1.3 Novelty

There are some novelty places in this thesis, as follows:

1. Direct metal deposition technology is used to fabricate the hardface layer and thermal stress control layer, this proposed technology can minimize inter-layers in the transition layer due to dilution layers in the vicinity of jointed regions.

2. The finite element simulation method is adopted for predicting the surface worn of the automobile axle die and designing thermal stress control layer between the hardened layer and the substrate.

3. Microstructure and properties of Stellite21 are researched by hardness tester, SEM, EDS and XRD devices.

Chapter 2 Theoretical basis for relieving thermal stress in hot forging dies

2.1 Hot forging die life and stress

The life of hot forging die is directly related to its load and stress state. To increase the service life of hot forging dies, it is necessary to understand the major failure modes and failure mechanisms of hot forging dies, and the specific relationship between the life of hot forging dies and thermal stress.

2.1.1 Failure modes of hot forging die

1. Mechanical wear

In the hot die forging process, the plastic deformation of the high temperature billet has violent metal flow related to the die surface. Due to the flow of billet on the die during forging process, the die surface can be ground, resulting in bluntness of the flange on the die and expansion of the die. In addition, the combined stress of shear stress and compressive stress during the metal flow process can shear the surface of the mold into small grooves, resulting in mechanical wear.

When the surface of the mold is oxidized, the mechanical wear of the mold is accelerated, especially when the temperature of a portion of the mold ridge is too high, the surface may be softened due to high temperature. In this case, in addition to the increased wear, the softened parts will also be “washed“ out of the larger grooves by the high-speed flow.

Wear will not only aggravate the surface quality of the die, but will also change size of the die. According to domestic and abroad, mechanical wear is

used in all scrap hammer forging dies and press dies. The amount of about 70%, of which the highest proportion of blunt[2].

2. Fatigue crack

Due to the various structure of forging dies, the stress state of each point on the forging die is also various. Under the action of cyclic mechanical loading, when the stress in some forging dies exceeds its fatigue limit, fatigue cracks will occur in the forging dies. To a certain degree of fatigue cracks, under the action of peak stress, the forging die is fatigued. Fatigue cracking is another major form of forging die damage, accounting for about 25% of the scrapped die[2].

Fatigue cracks are likely to occur at the corners of the mold subjected to large bending moments (the direction of its extension and impact is 45°) and partial cracks will appear on the sidewalls of the circular section molds and at the bottom of the molds.

3. Thermal fatigue crack

The surface of the mold is periodically heated and cooled for the forging production process, and the internal heat is subjected to tensile and compressive heat alternating stress, so that an interstitial crack (crystal crack) and local deformation are generated in the microstructure of die. These tiny cracks, namely thermal cracking, most of which occur in the mold where the flow of deformed metal is slow.

4. Plastic deformation

A part of a mold where deformed metal flows at high speed can be softened due to the severe frictional heat effect or the die (such as convex platform) is softened by the hot metal. It causes plastic deformation under the

action of high temperature and pressure. In addition, during the forging process, the mold wall will also be plastically deformed if the strength of the mold steel is insufficient for thermal soften.

5. Brittle failure

When the forging die is overloaded, equipment failure, violation of the process specification and internal defects of the mold material will cause brittle failure, brittle failure is an “accident“, and should be avoided as much as possible. Studies have shown that mechanical wear and fatigue cracks account for most of the failure of hot forging dies[15,16,17].

2.1.2 Relationship between life and stress of hot forging die

In the hot forging process, the mold is subjected to alternating thermal load in addition to the mechanical load. During the loading, the surface temperature of the die cavity increases dramatically, and then decreases rapidly after unloading. The transient temperature peak phase is very short. Thermal loads only affect the surface layer of the die cavity that is extremely thin. With the rapid change of the surface temperature of the cavity, each point of die cavity affected by temperature will produce a corresponding deformation, and the corresponding point of die cavity will generate tensile and compressive stress due to the constraint of the surrounding point. When the stress value exceeds the allowable fatigue limit of the mold material, thermal fatigue cracks will occur. When the transient temperature of the mold exceeds the phase transition temperature of the mold material, the surface metal phase changes, which not only reduces the mechanical properties of the mold material, but also accelerates the wear of the mold material. It can be seen that periodic thermal shock loads and stresses have a direct impact on the life of the mold.

The fatigue failure of the part starts from the maximum local strain, so the starting point of the local stress-strain analysis method is used to predict the life of the die. A certain plastic deformation is required before the small crack initiation, and the local plastic deformation occurs. It is a prerequisite for initiation and expansion of small fatigue cracks. Therefore, it is the maximum local stress and strain that determines the fatigue strength and life of components. As long as the maximum local stress and strain are the same, the fatigue life is the same. The fatigue damage of hot forging die belongs to low cycle thermal fatigue, and the basis of local stress-strain analysis is low cycle fatigue. The fatigue life in low cycle fatigue refers to the crack formation life. The expression of the fatigue life curve used in the local stress-strain analysis method is the Manson-Coffin equation[18]. The low cycle fatigue life prediction method was independently proposed by Coffin and Manson on the basis of experiments, this method can be well matched with the test results[19].

The thermal load and mechanical load of the hot forging die are asymmetrical. According to the fatigue strength theory, the working safety factor of the component under asymmetrical cycle n_σ[20].

$$n_\sigma = \frac{\sigma_{-1}}{\frac{K_\sigma}{\xi_\sigma \beta}\sigma_A + \psi_\sigma \sigma_M} \tag{1}$$

where σ_{-1}, σ_A, σ_M are the fatigue limits of the component materials, the average stress of the asymmetrical component, and the stress amplitude; K_σ, ξ_σ, β are the effective stress concentration factor of the component, the size factor, and the surface quality factor; ψ_σ is the sensitive factor of component material.

From the above equation, we can take the following remedies:

(1) Select a higher fatigue limit of hot die material;

(2) Reduce the stress amplitude of the mold during hot forging;

(3) Reduce the average stress of the mold during hot forging.

When the used temperature of the hot forging die varies between 200~700℃, the sensitivity factor ψ_σ of the hot forging die material generally varies between 0~0.25, and the value of $\frac{K_\sigma}{\xi_\sigma \beta}$ is generally between 2~3[20]. The average stress σ_M of forging dies relative to the stress amplitude σ_A of the forging dies has little effect on the working safety factors of the forging dies. Especially when the cavity surface temperature is the highest at the end of the forging, the average stress of the forging dies can be ignored. Only the impact of stress amplitude of the forging die is considered for the safety factors. It can be seen that the stress amplitude of the mold during hot forging must be reduced to increase the life of the mold.

The stress of the hot forging die during work is the synthesis of thermal stress and mechanical stress. Through the open die forging process and the overall optimized design of the die flash size to reduce the mechanical load and mechanical stress, it can play a role in improving the life of the die. However even if a very comprehensive measure is taken to reduce the machine load, the effect of increasing the life of the forging die is also very limited. This is because the mechanical stress only occupies a small part of the overall stress of the mold, and thermal stress is the main body of the comprehensive stress of the mold. Therefore, to improve the life of the mold, the most important thing is how to relieve the thermal stress amplitude of the hot forging die.

2.2 Temperature distribution and heat transfer characteristics of die

The heat load of the forging die comes from the heat conduction when the die cavity surface is in contact with the billet and the frictional heat effect produced when the billet slips along the surface of the die cavity. The temperature value of cavity surface is related to the heating temperature of the billet, the preheating temperature of the mold, the cooling and lubrication conditions, and also relates to the contact stress, the contact time, and the deformation speed of the billet in the cavity. For a single forging, the thermal load acts on the surface of the die cavity in a pulsed manner, while in the continuous forging, it periodically acts on the surface of the die cavity in a pulsed manner.

According to the test results, the heat load on the forging die mainly affects the loaded state and service life of the die surface and the near surface layer. Therefore, this article pays attention to the temperature distribution and heat transfer characteristics of the die surface and the near surface layer. Because the thickness of the near surface layer is approximately infinite compared with the overall size of the mold, the above problem can be approximated as a one-dimensional heat transfer problem of a semi-infinite object. The heat conduction of the mold is equivalent to the surface contact heat transfer of a semi-infinite object. Frictional heat generation is equivalent to the heat conduction problem of a constant heat source on the surface of a semi-infinite object.

2.2.1 Heat transfer

(1) Heat transfer differential equation

According to the theory of heat transfer, the differential equation for the one-dimensional unsteady heat conduction problem is:

$$\frac{\partial T(x,t)}{\partial t} = a\frac{\partial^2 T(x,t)}{\partial x^2} \tag{2}$$

where T(x,t): temperature function (℃);

a: thermal diffusivity (m^2/s) ;

t: time (s);

x: position coordinates (m).

As shown in Figure 2-1, the following mark "1" represents the relevant parameters of the metal billet, the lower mark "2" represents the relevant parameters of the die, and the contact surface of the die and the forging is the coordinate zero point, then:

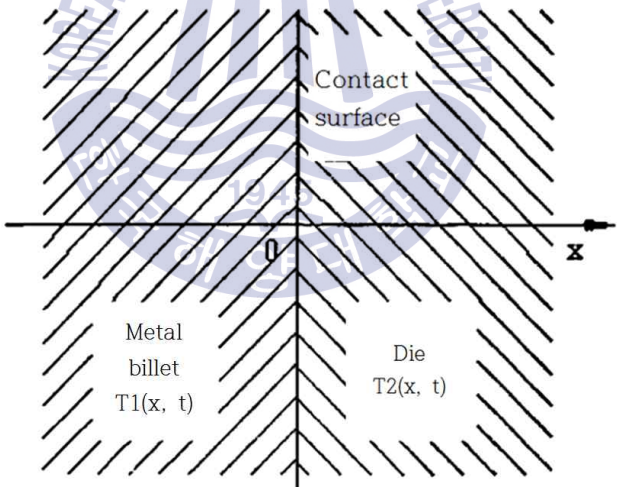

Fig. 2-1 The contact diagram between the billet and the mold

$$\frac{\partial T_1(x,t)}{\partial t} = a_1\frac{\partial^2 T_1(x,t)}{\partial x^2} \tag{3}$$

$$\frac{\partial T_2(x,t)}{\partial t} = a_2\frac{\partial^2 T_2(x,t)}{\partial x^2} \quad (t>0, x>0) \tag{4}$$

(2) Initial conditions and boundary conditions

$$T_1(x,0)=T_{10,} \qquad T_2(x,0)=T_{20} \tag{5}$$

$$\lambda_1\frac{\partial T_1(0,t)}{\partial x}=-\lambda_2\frac{\partial T_2(0,t)}{\partial x}, \quad \frac{\partial T_1(-\infty,t)}{\partial x}=\frac{\partial T_2(+\infty,t)}{\partial x}=0 \tag{6}$$

$$T_1(0,t)=T_2(0,t) \qquad (t>0) \tag{7}$$

where T_{10}: forging starting temperature of metal billet (℃);

T_{20}: preheating temperature of mold (℃);

λ_1, λ_2: thermal conductivity of metal billet and molds (W/m・℃).

(3) Temperature distribution of surface layer of forging model cavity

Using the initial conditions and boundary conditions to solve the differential equation (3) and the equation (4), the temperature distribution function of the mold cavity surface layer is obtained as:

$$T_2(x,t)=\frac{T_{10}-T_{20}}{1+\frac{\lambda_2}{\lambda_1}\sqrt{\frac{a_1}{a_2}}}erfc[x/(2\sqrt{a_2t})] \tag{8}$$

where erfc(x): the residual error function of the argument x, $erfc(x)=\frac{2}{\sqrt{\pi}}\int_x^{+\infty}e^{-t^2}dt$, Its relationship with the error function erfc(x) is erfc(x)=1-erf(x).

The temperature distribution function of the surface layer of the forging cavity caused by the heat conduction of metal billet is made by $T_d(x, t)$, $k=1/(\frac{\lambda_2}{\lambda_1}\sqrt{\frac{a_1}{a_2}})$, and combined with erfc(x)=1–erf(x):

$$T_d(x,t)=k(T_{10}-T_{20})+k(T_{20}-T_{10})erf[x/(2\sqrt{a_2t})] \tag{9}$$

(4) Surface temperature of cavity

$$T_d(0,t) = k(T_{10} - T_{20}) \tag{10}$$

When the forging material and the mold material are determined, the temperature of the cavity surface is only proportional to the difference between the billet initial forging temperature and the mold temperature.

(5) Time domain characteristics of transient temperature of cavity surface layer

The temperature curve of the surface layer of the mold cavity is drawn according to equation (9), it is shown in Fig. 2-2. From the figure, it can be seen that with the increase of x, the increasing amplitude of temperature gradually decreases along the thickness direction of the mold, and the temperature increase begins to delay with the appearance time of the peak temperature, which is consistent with the experimental test results.

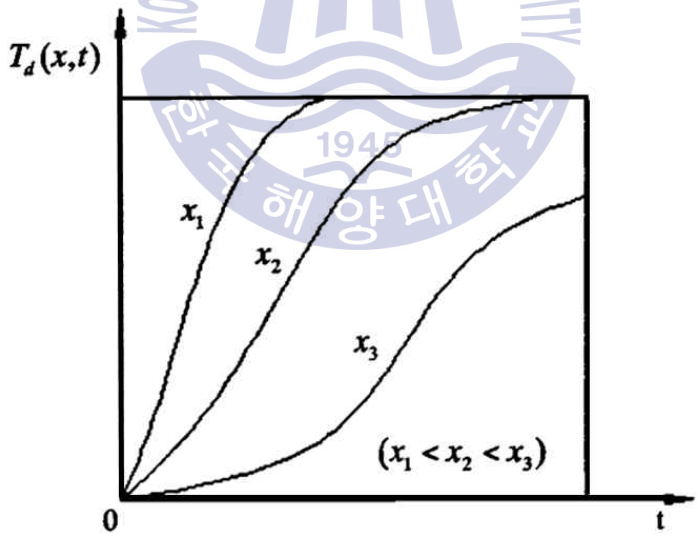

Fig. 2-2 The temperature time curve of mold surface[3]

According to equation (9), at any time t, the position $X_{0\%}$ at which the temperature rise in the mold starts can be obtained by the following equation:

$$erf(\frac{x}{2\sqrt{a_2 t}}) = 1.0 \tag{11}$$

$so, \qquad x_{0\%} = 4\sqrt{a_2 t}$

In general forging production, the contact time between the metal billet and the mold cavity is approximately tens of milliseconds to several seconds. In such a short time, the heat affected zone of the surface layer of the mold cavity is only a few millimeters thick.

2.2.2 Heat conduction by frictional heat generation

(1) Heat transfer differential equation

By equation (4),

$$\frac{\partial T_2(x,t)}{\partial t} = a_2 \frac{\partial^2 T_2(x,t)}{\partial x^2} \tag{12}$$

$$\frac{\partial q(x,t)}{\partial t} = a_2 \frac{\partial^2 q(x,t)}{\partial x^2} \tag{13}$$

$$\frac{\partial}{\partial t}[\frac{\partial T_2(x,t)}{\partial x}] = a_2 \frac{\partial^2}{\partial x^2}[\frac{\partial T_2(x,t)}{\partial x}] \tag{14}$$

$$q(x,t) = -\lambda_2 \frac{\partial T_2(x,t)}{\partial t} \tag{15}$$

$$\frac{\partial q(x,t)}{\partial t} = a_2 \frac{\partial^2 q(x,t)}{\partial x^2} \tag{16}$$

(2) Initial conditions and boundary conditions

$q(x,0) = 0, \quad q(0,t) = q_c, \quad q(\infty,t) = 0,$

where q_c: the constant heat flux (W/m^2) caused by the friction between the

metal billet and the mold cavity. As the heat source transfers heat to the billet and the mold at the same time, the equation is calculated according to the heat flow distribution coefficient:

$$a_{hf} = \sqrt{\lambda_2 c_2 \rho_2} / (\sqrt{\lambda_1 c_1 \rho_1} + \sqrt{\lambda_2 c_2 \rho_2}) \tag{17}$$

so, $q_c \approx \frac{1}{2} \mu p \nu$;

μ: the friction coefficient of the contact between the metal billet and the mold cavity;

p: normal stress at the contact between the metal billets and the mold cavity(N/m^2) ;

c_1, c_2: specific heat of metal billets and forging dies(J/Kg · ℃) ;

ρ_1, ρ_2: density of metal billets and forging dies(Kg/m^3);

ν : sliding speed (m/s) of the metal billet along the cavity surface(m/s).

(3) Temperature distribution of surface layer of forging model cavity

Using the initial conditions and boundary conditions to solve the differential equation (16), the heat flux distribution function of the surface layer of the mold cavity is:

$$q(x,t) = q_c erfc(\frac{x}{2\sqrt{a_2 t}}) \tag{18}$$

Substituting it into equation (15) and integrating from x to + ∞:

$$T_2(x,t) = \frac{q_c}{\lambda_2} \int_x^{\infty} erfc(\frac{x}{2\sqrt{a_2 t}}) dx = \frac{2q_c}{\lambda_2} \sqrt{a_2 t} \cdot ierfc(\frac{x}{2\sqrt{a_2 t}}) \tag{19}$$

where ierfc(x): the residual error function of the independent variable X[21]. Let $T_m(x,t)$ be the temperature distribution function of the surface layer of the forging die caused by frictional heating between the metal billet and the

mold cavity surface:

$$T_m(x,t) = \frac{\mu p \nu}{\lambda_2}\sqrt{a_2 t} \cdot ierfc(\frac{x}{2\sqrt{a_2 t}}) \tag{20}$$

(3) Cavity surface temperature:

$$T_m(0,t) = \frac{0.5642\mu p \nu}{\lambda_2}\sqrt{a_2 t} \tag{21}$$

Cavity surface maximum temperature:

$$T_{\max} = T_d(0,t) + T_m(0,t) + T_{20}$$

then: $$T_{\max} = kT_{10} + (1-k)T_{20} + \frac{0.5642\mu p \nu}{\lambda_2}\sqrt{a_2 \tau} \tag{22}$$

where, τ : contact duration (s) of contact between the billet and the cavity surface during deformation of the metal billet.

$k = 1/(1 + \frac{\lambda_2}{\lambda_1}\sqrt{\frac{a_1}{a_2}})$, For common die forging steel parts, the value of k ranges from 0.5 to 0.55. In general analysis, it takes k=0.54.

p: the normal stress at the contact between the metal billet and the mold cavity, because the contact surface of the metal billet and the mold cavity is not ideally smooth, the part of the forging pressure on the surface of the mold cavity is only a few points or a small area of the surface protrusion. It can be remembered $p=n\sigma_s$ in the different stages of the forging forming process, n takes the corresponding value.

μ: the friction coefficient between the metal billet and the mold cavity surface, according to the Coulomb friction theorem, μ should be constant on the friction surface, but there is no such friction coefficient in actual hot deformation. Considering the type of forging materials and the use of lubricants in the actual forging process, μ = 0.18~0.5 is often used.

(4) Time domain characteristics of transient temperature of cavity surface layer

The temperature curve of the surface layer of the mold cavity drawn according to equation (20) is shown in Figure 2-3. As can be seen from the figure, with the prolonged deformation time of the metal billet, the surface temperature of the mold cavity rapidly increases, but the temperature change range far from the mold cavity surface layer is not large, which is consistent with experimental test results. The increase in temperature gradually decreases, and the increase in temperature begins to delay with the appearance of the peak temperature, which is consistent with the experimental test results.

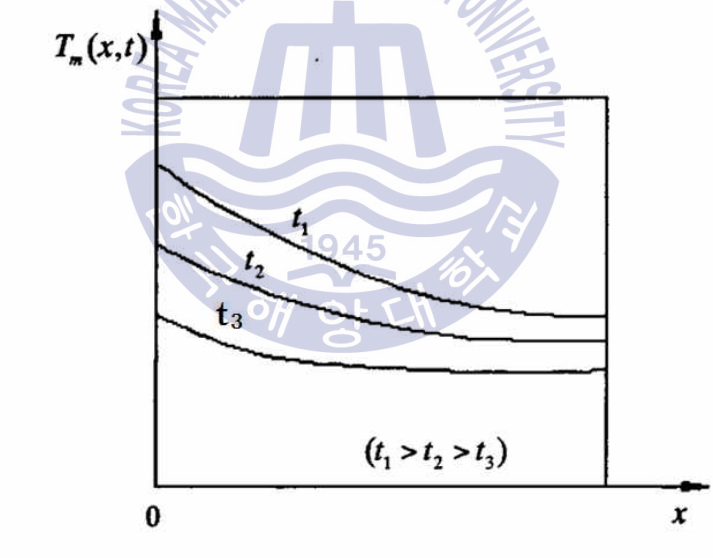

Fig. 2-3 Temperature distribution curve of mold surface[3]

From equation (9), at any time t, the position x_1 at which the temperature rise in the mold starts can be obtained from the following equation:

$$ierfc(\frac{x}{2\sqrt{a_2 t}}) \approx 0$$

Check the table from book:[21] $\frac{x}{2\sqrt{a_2 t}} = 1.6$

In general die forging production, the transient temperature rise caused by friction factors only affects the thickness of the surface layer of the mold cavity to several millimeters thick.

2.2.3 Temperature difference between mold surface layer and near surface layer

The fundamental reason for the tensile and compressive stress of the mold surface layer is that there is a temperature gradient between the surface layer and the near surface layer of the mold. The peak of compressive stress is related to the peak temperature of the mold surface layer and the average temperature of the near surface layer. The peak tensile stress is related to the propagation characteristics of the various harmonics of the temperature signal in the mold, its value depends on the average value of the surface layer temperature and the peak value of the near-surface layer temperature. The peak temperature difference between the surface layer and the near surface layer of the die when using the die forging equipment corresponding to various types of temperature pulse signals is as follows:

(1) Sawtooth-like signals such as high-speed hammers in a continuous blow

$$(\triangle T)_{\min} = -\frac{0.2}{\pi} T_{\max} \qquad (23)$$

$$(\triangle T)_{\max} = \frac{1}{2} T_{\max} \tag{24}$$

(2) A triangular wave signal such as a hammer, etc. in a continuous blow

$$(\triangle T)_{\min} = -\frac{0.8}{\pi^2} T_{\max} \tag{25}$$

$$(\triangle T)_{\max} = \frac{1}{2} T_{\max} \tag{26}$$

(3) Sinusoidal signals such as die forging presses in a continuous blow

$$(\triangle T)_{\min} = -\frac{0.8}{3\pi} T_{\max} \tag{27}$$

$$(\triangle T)_{\max} = \frac{1.14}{\pi} T_{\max} \tag{28}$$

2.3 Theoretical expression of peak thermal stress in hot forging die

According to the deformation characteristics of the mold cavity, it can be considered that the stress state of the cavity surface is a plane stress state. Since the temperature function of the mold working surface is periodically changed, the functions of temperature, displacement and stress are expanded into Fourier series. The form is calculated to give the thermal stress wave distribution function at the depth (z-direction) of the mold cavity surface [22]:

$$\sigma_w = \frac{E\alpha}{1-\nu} \triangle T \exp(-z\sqrt{\frac{w}{2a}}) \cos(z\sqrt{\frac{w}{2a}}\, wt) \tag{29}$$

where E: the elastic modulus of the mold material;

α : linear expansion coefficient of mold material

a: temperature coefficient of mold material;

ν : poisson's ratio of mold materials;

△T: the temperature difference between the surface layer and the

near surface layer at the danger point of the mold;

w: the harmonic frequency of the thermal stress function.

Therefore, the equations for calculating the peak values of tensile and compressive stress at the dangerous points on the surface layer of the mold are as follows:

$$\sigma_{\min} = -\frac{E\alpha(\triangle T)_{\min}}{1-\nu} \tag{30}$$

$$\sigma_{\max} = -\frac{E\alpha(\triangle T)_{\max}}{1-\nu} \tag{31}$$

$(\triangle T)_{min}$,$(\triangle T)_{max}$ are the minimum and maximum values of the temperature difference between the surface layer and the near surface of the mold cavity respectively.

(1) Fatigue characteristic parameters at the dangerous point of the mold surface layer

Cyclic thermal stress average:

$$\sigma_m = \frac{\sigma_{\max} + \sigma_{\min}}{2} \tag{32}$$

Thermal stress amplitude :

$$\sigma_a = \left|\frac{\sigma_{\max} - \sigma_{\min}}{2}\right| \tag{33}$$

Thermal stress characteristic parameters:

$$Y = \frac{\sigma_{\min}}{\sigma_{\max}} \tag{34}$$

(2) Parametric expression of peak thermal stress in hot forging die

In order to illustrate the convenience of the problem, taking the die forging

of a continuous hot die forging press as an example, the parameter expressions of the peak thermal stress and the cyclic thermal stress amplitude at the dangerous point on the surface of the hot forging die are listed.

The equations for calculating the peak values of tensile and compressive stress at the dangerous points on the surface layer of the mold by substituting (18) and (19) into (21) and (22) are respectively as follows:

$$\sigma_{\min} = \frac{0.8E\alpha}{3\pi(1-\nu)}[T_y + k(T_d - T_y) + 0.5642\mu pv\sqrt{\frac{\tau}{\rho\lambda c}}] \tag{35}$$

$$\sigma_{\max} = -\frac{1.14E\alpha}{\pi(1-\nu)}[T_y + k(T_d - T_y) + 0.5642\mu pv\sqrt{\frac{\tau}{\rho\lambda c}}] \tag{36}$$

The equation for the circulating thermal stress amplitude is as follows:

$$\sigma_a = \frac{5.02E\alpha}{6\pi(1-\nu)}[T_y + k(T_d - T_y) + 0.5642\mu pv\sqrt{\frac{\tau}{\rho\lambda c}}] \tag{37}$$

Among, p=n σ_s , $K = 1/(1+\sqrt{\frac{\rho_m\lambda_m c_m}{\rho_d\lambda_d c_d}})$,

$$\tau = \frac{30}{\pi N_0} arccos[1 - \frac{2(\triangle H + F_1)}{H}] + \arccos(1 - \frac{2F_1}{H}) \tag{38}$$

According to the influence parameters in the equation, the methods and measures to relieve the thermal stress of the hot forging die can be theoretically directed. In fact, due to the limitation of process conditions, some parameter adjustment ranges are very limited. For example, initial temperature parameters T_y and T_d, some parameters cannot be precisely controlled and detected, such as the friction factor μ at the contact between the billet and the die cavity, and some effects are very limited. Taking this actual situation into consideration, the thermal stress of hot forging die is relieved from the following four manners.

1. Reduce the temperature difference between the surface layer and the

near surface layer of the dangerous point of the mold cavity△T;

2. Use better hot forging die materials:

3. Develop and use new functional materials;

4. Improve process parameters.

Chapter 3 Prediction of wear region of axle die by finite element method

In forging, die failure can be a significant portion of the overall production cost. The cost to replace a die includes the basic cost of the die, which encompasses the cost of material, machining, coating, and surface treatment as well as the cost of labor. In any case, the most important cost of die failure is related to the down-time of the manufacturing system, which reduces the overall productivity[23]. Therefore, to remain competitive, the cost-effective application of computer aided techniques, i.e. CAD, CAM, CAE and especially Finite Element Analysis (FEA) and Finite Volume Analysis (FVA) based computer simulation, are an absolute necessity. Figure 3-1 shows the application procedure of CAD, CAD, CAM, CAT. The practical use of these techniques requires knowledge of the principal variables of the forging process and their interactions. These variables include: a) the flow behavior of the forged material under processing conditions, b) die geometry and materials, c) friction and lubrication, d) the mechanics of deformation, i.e. strains and stresses, e) the characteristics of the forging equipment, f) the geometry, tolerances, surface finish and mechanical properties of the forging, and g) the effects of the process on the environment[24].

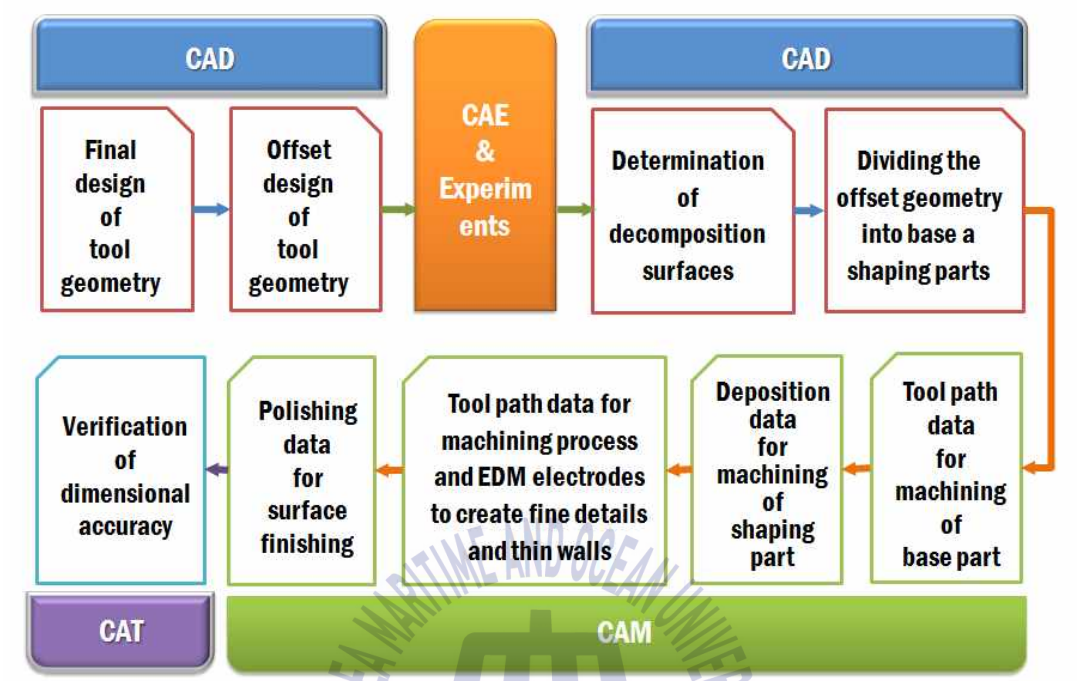

Fig. 3-1 Application procedure of CAD/CAM/CAT

The finite element method has gained wide acceptance in the industry and academia. This can be attributed to the rapid advancement in the computing technology, user-friendly commercial FE software and detailed information FEM can provide as compared to other methods of analysis, the FE method allows the user to incorporate in the simulation: (a) the tool and workpiece temperature, (b) the heat transfer during deformation, (c) strain-rate-dependent material properties, (d) strain hardening characteristics, and (e) capabilities for microstructure analysis. This results in a more accurate analysis of the forging process. Commercial FE software packages have been used successfully in simulating complex two-dimensional (2-D) and three-dimensional (3-D) forging operations. In this chapter, the hot forging die of axle shaft is researched by the way of finite element simulation, the

worn region of the die is predicated, the harden layer is designed and the thermal stress at the interface between the deposition layer and the substrate is analyzed.

3.1 Axle forging

Automobile axle shaft should be subjected to a number of complex stresses during working, such as rotational bending and impact. Fatigue cracking is main form of failure. Therefore, the axle material is required to have sufficient strength and toughness, and manufacturing process is very strict. In general, axles are manufactured by hot forging process. The plastic deformation resistance of metal directly affects the quality of the forgings made of metal billet and tool life. Billet is heated before forging, the main purpose is to enhance the plasticity and reduce the deformation resistance so as to get a good workpiece after forging. The axle shaft mainly adopts the heating method of the step-type continuous heating furnace. Figure 3-2(a) shows the heating of the workpiece.

Dies for forging steel and other metals that must be forged at high temperatures are susceptible to heat checking, or the development of minute cracks in the die surface[25]. Heat checking appears mainly in corners or on ledge of the die. It occurs when the die surface has become overheated while the center of the block remains relatively cool. The variation in rates of contraction on cooling causes the surface to crack. Once cracks are started, forging forces (specially the forces of impact) will cause cracks to grow, and if this is allowed to continue, die breakage will result. Most heat checking occurs in the forging of steel and heat-resisting alloys, considerably less in the forging of copper alloys, and little in the forging of aluminum or magnesium alloys, because of work-metal temperature. In this paper, the material of hot forging die is SKD61, a kind of hot working die steel. So, hot

forging die is heated before starting to work as shown in Figure 3-2(b).

Figure 3-2(c) shows the production equipment of an axle forge. The heated forgings are rapidly placed on the production equipment, this is to prevent the temperature drop and oxidization of the workpiece, it will affect plastic deformation of workpiece. Figure 3-2(d) shows the shape of workpiece after forging. After the workpiece is forged, allow it to cool naturally to room temperature. This will ensure that the residual stress in the material is less.

Fig. 3-2 Manufacturing process of axle shaft: (a) Heating of the workpiece; (b) Preheat treatment of die; (c) Production equipment of an axle forge; (d) Shape of workpiece after forging

3.2 Three-dimensional model

In metal forming processes, both plastic deformation and friction contribute to heat generation. The temperatures developed during the forging operation influence tool life, as well as microstructure and properties of the forging part. With the finite element based process modeling, the heat generation during deformation and heat transfer before, during, and after deformation can all be calculated in a computer. To ensure accurate heat transfer calculation, correct work-piece and die interface heat transfer coefficient must be known. Using accurate process modeling, the influence of press speed, connect time, and heat transfer in metal forming can be evaluated.

Figure 3-3(a) shows the geometric model of the forging die of the automobile axle. The left figure shows the entire model of the grinding tool, and the right side is the section of the model. From the right side figure, the internal dimension of the model can be clearly seen. The dimension of the model is according to the actual size of the factory one to one established. The axle's hot forging tool is a cylinder and an axisymmetric pattern. Accuracy of simulation results and calculation time are relative to number and size of grids, the number and size of grids of model is determined the volume of model. In order to save the calculation time and improve the accuracy of simulation results, a quarter model is used for simulation calculation. Figure 3-3(b) is a quarter-finite model used for simulation calculations and meshes the model. It can be seen from the figure that the model surface, edges and corners, as well as the raised parts are densely meshed, it is to improve the accuracy of the calculation results.

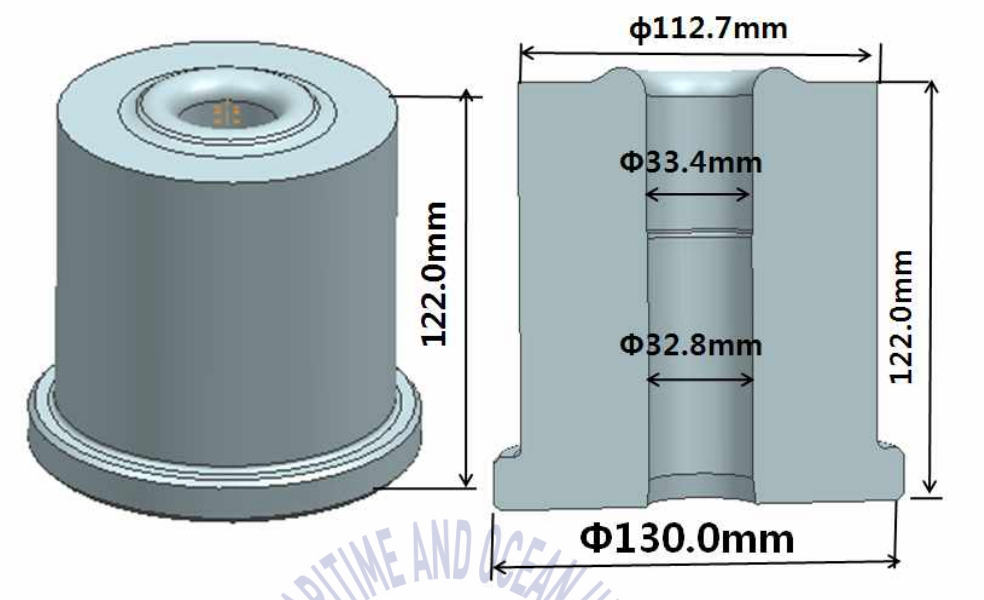

(a) Geometry model

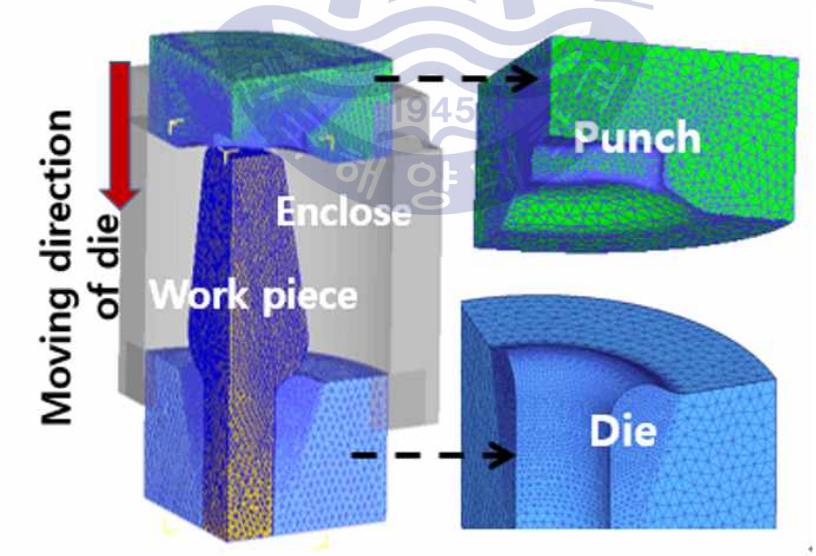

(b) Finite element model

Fig. 3-3 Design model for analysis

3.3 Properties of SKD61 and Stellite21

Die material and hardness have great influence on die life. A die made of well-chosen material at the proper hardness can withstand the severe strains imposed by both high pressure and heavy shock loads, and can resist wear, cracking and heat checking.

SKD61 is a kind of hot forging steel with excellent strength, toughness and heat resistance balance. It is a medium-alloy hot forging steel containing silicon, chromium, molybdenum, and vanadium. Its chemical composition is shown in Table 3-1 and physical properties in Table 3-2. This years, with the development of isotropic products, it is increasingly developing in high toughness and high hardness. It can make the life of hot forging die longer. The performance is more stable and easy to process. However, this still cannot meet the human needs for its use. Under high temperature working, its hardness will rapidly decrease, the working life of die made by SKD61 would also reduce.

Many types of hard material can be coated on surfaces to improve wear resistance, strength, and corrosion characteristics. Cobalt superalloys, Nickel-base superalloy and Iron-base superalloy are commonly hardfacing materials. Stellite21 is a kind of Cobalt superalloys, its chemical composition contains a lot of alloying element and less carbon content so that it has a good hardness and toughness at high temperature. In addition, Stellite21 has several unique properties, such as creep-resistance and abrasive resistance, bio-compatibility, and corrosion resistance. with the welding technology development, Stellite21 coatings have been developed by various techniques[26-34], for example, plasma transferred arc (PTA) welding and high power diode laser (HPDL) cladding. So, it is used as hardfacing material for axle's forging die. The chemical composition of Stellite21 is given in Table

3-1 and its mechanical and physical properties in Table 3-2.

Table 3-1 Chemical composition (wt%) of SKD61 and Stellite21

	C	Si	Mn	P	Cr	Mo	V	Fe	Co
SKD61	0.32~0.42	0.08~1.2	0.5	0.03	4.5~5.5	1~1.5	0.8~1.2	Bal	—
Stellite 21	0.2~0.35	1.3	1	—	26~29	4.5~6	—	3.5	Bal

Table 3-2 Typical values of mechanical and physical properties of SKD61 and Stellite21 at room temperature

Mechanical and physical properties	SKD61	Stellite 21
Hardness (HV)	420	450
Modulus of elasticity (GPa)	200	245
Thermal conductivity (W/m·℃)	25	17
Density (kg/m^3)	7760	8330
Specific heat (J/kg·℃)	460	423
Thermal expansion coefficient (10^{-6}/K)	10.4	14.3
Poisson's ratio	0.29	0.3

During the forging process, the surface temperature of the hot forging die increases so that thermal softening of the die surface material, thereby causing rapid wear of the die. Therefore, the strength of the mold material at high temperatures directly affects the wear resistance of the mold. Figure 3-4 shows the hardness of the Stellite21 and SKD61 at high temperature. It can

be seen from the figure that the hardness of Stellite21 and SKD61 decreases as the temperature increases, but the hardness of Stellite21 decreases more slowly than that of SKD61. In other words, the Stellite21 can maintain a good mechanical property even at high temperatures.

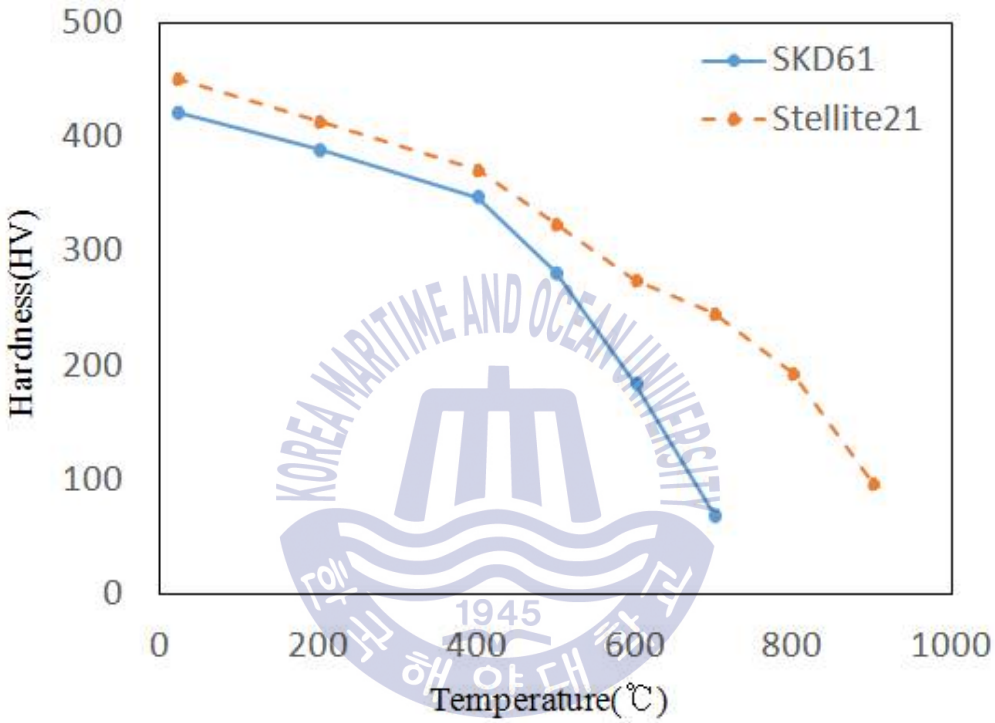

Fig. 3-4 Hardness of Stellite21 and SKD61 at high temperature

3.4 Initial simulation parameters

After the simulation model is established, the boundary conditions and corresponding simulation parameters should be set for the model. The simulation process parameters must be consistent with the actual production conditions of the factory, since only this way can ensure that the simulation results are consistent with the actual. When the axle of the automobile is forged, the forging speed of the abrasive tool is 400 mm/s. The moving

distance of top die is 67mm, the initial temperature of workpiece is about 1150° C. In order to improve the performance of the hot forging die and avoid hot checking, the forging die are preheated, and the temperature of the forging die after preheating is about 350° C. This method can well prevent the occurrence of heat cracks on the surface of the forging die. The working temperature is about 30° C. The heat conductivity in the forging die is 2 W/m^2 · ° C, while the heat conductivity between the tool and the workpiece is 11 W/m^2 · ° C and the friction coefficient is 0.7. Tables 3-3 and 3-4 shows simulation data for model analysis.

Table 3-3 Simulation data for wear analysis

Object type	Workpiece : Plastic Die : Rigid
Initial temperature of object	Workpiece : 1150℃ Die : 350℃
Die speed [mm/s]	420
Die pressing depth [mm]	67
Heat transfer coefficient on bottom die [W/m^2 · ℃]	2

Table 3-4 Interface properties between workpiece and dies

Object relationship	Friction factor	Heat transfer coefficient [W/m^2 · ℃]
Punch-workpiece	0.6	11
Die-workpiece		

The manufacturing material of the axle hot forging die is SKD61, a commonly used hot forging tool steel, and its specific chemical composition is shown in Table 3-1. Table 3-5 shows the thermal physical properties of SKD61.

Table 3-5 Thermal physical properties of SKD61 and Stellite21

Properties	SKD61		Stellite21	
	Temperature [℃]	Value	Temperature [℃]	Value
Young's modulus [GPa]	25	200	25	245
	649	113.8	649	191.7
	760	103.6	760	182.2
	1150	68.9	1150	149
Thermal expansion [10^{-6}mm/mm · ℃]	100	10.4	427	14.3
	425	12.2	649	15.1
	650	13.1	816	15.6
	1370	13.86	2000	28
Thermal conductivity [W/m^2 · ℃]	20	25	20	17
	350	28.4	300	18.8
	605	28.7	600	24.2
Specific heat [J/kg · ℃]	460		423	
Density [kg/m^3]	7760		8330	
Poisson's ratio	0.29		0.3	

3.5 Archard wear model

Some of analytical wear models are developed by Holm, Archard, and Rabinowicz. Among them, Archard model is often used in the model analysis. Archard's model is applied to analytical wear models in DEFORM software. Information from the manufacturing process of an axle should be put into the 3D-DEFORM. This wear model is expressed as Eq. (30) [35-37]:

$$W = \int_{t_1}^{t_2} K \frac{P^a V^b}{H^c} dt \tag{39}$$

where W is the wear volume of die. P is the interface pressure, v is the sliding velocity, H is the hardness of tool material, dt is the time increment, a, b, c, K is the experimentally calibrated coefficients (a, b are commonly taken as 1, and c = 2 for tool steels)[38]. According to the equation, the wear volume of die is related to interface pressure, sliding velocity, contact time, friction coefficients and hardness of material. It is recognized very clearly that adhesive and abrasive die wear can be minimized by reducing the wear coefficient, the normal pressure and the sliding length and by increasing the die hardness. Table 3-6 is the hardness and wear coefficient of SKD61 at the high temperature[14].

Table 3-6 Input data for wear analysis

Properties	Temperature [℃]	Value
Hardness of die [HV]	300	370
	500	281.7
Tool wear coefficient [10^{-6}]	300	17.3
	500	26.1

3.6 Simulation results

3.6.1 Simulation results of conventional die

In hot forging, the workpiece is a continuous change process, the forging pressure is gradually increasing with the contact area increase between the workpiece and die. Figure 3-5 shows the change of pressure during the

forging process with time. From the figure, it can be seen that the entire forging process requires about 0.161 s and the maximum pressure is about 1.28×10^6 N. Figure 3-6 shows the shape change process of the workpiece during the forging process. It can be seen from the figure that the contact area between the workpiece and the bottom die gradually becomes larger, so the pressure required for forging increases gradually.

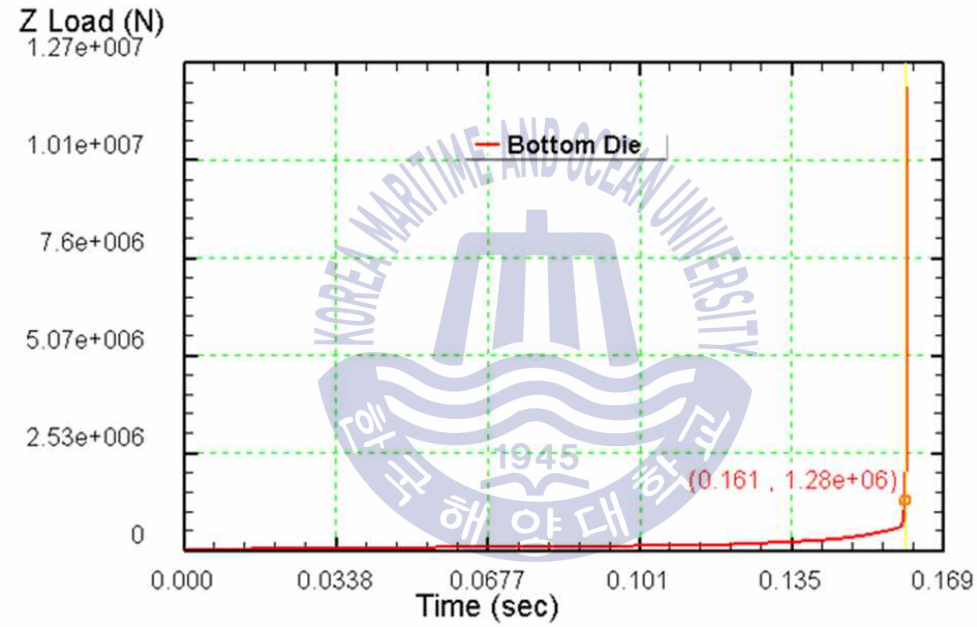

Fig. 3-5 Load-time curve of conventional during forging process

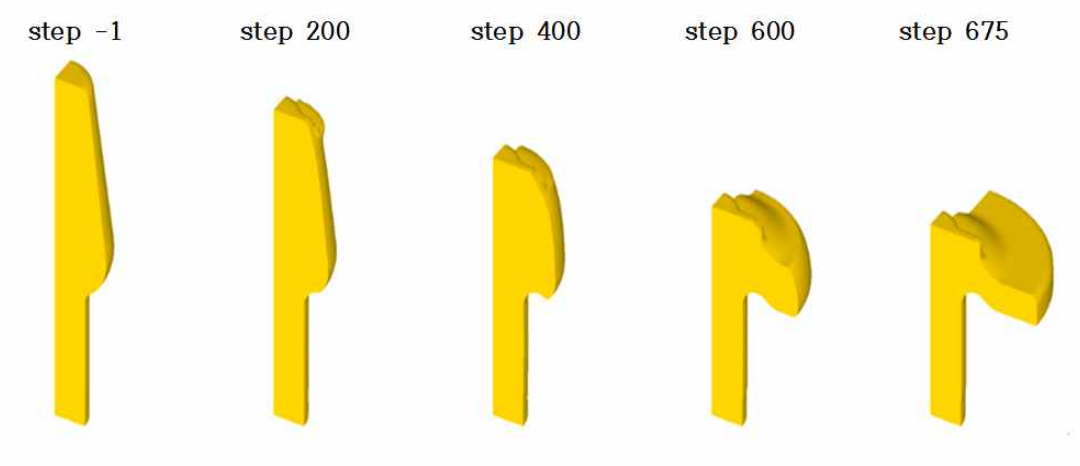

Fig. 3-6 Deformed shape of workpiece

Figure 3-7 shows the temperature distribution on the workpiece, It can be seen from the figure that after hot forging process, the maximum temperature of the workpiece is higher than initial temperature, this is because internal metal atoms rub against each other during deformation. The greater the deformation, the higher the temperature.

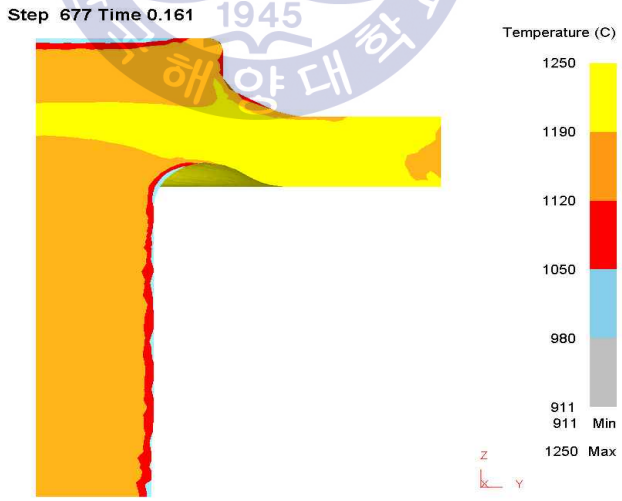

Fig. 3-7 Temperature distribution on the workpiece

Figure (3-8) to (3-10) show the variation and distribution of the interface temperature, interface pressure, and slipping velocityon the hot forging tool during forging of the axle. It can be seen from the figure that the maximum temperature of the surface is 894° C and it appears on the top of the convex portion. During the entire forging process, the convex portion of the abrasive tool is the highest. Therefore, the hardness of this portion of the material is reduced and it is prone to wear. The maximum sliding velocity is 734 mm/s, appearing on the top surface of die, but the maximum sliding velocity is always appearing on the top of the convex portion during the whole forging process. The maximum interface pressure is 791 MPa. The maximum interface pressure occurs at the top to the inside of the bulge. According to the classic Archard model, the largest position of abrasive wear should be the convex top. Figure 3-11 shows the surface wear map of the abrasive tool. The largest part of the wear appears on the top of the bulge. Therefore, the hardened area of the abrasive tool is selected as the convex portion, it is shown in Figure 3-11.

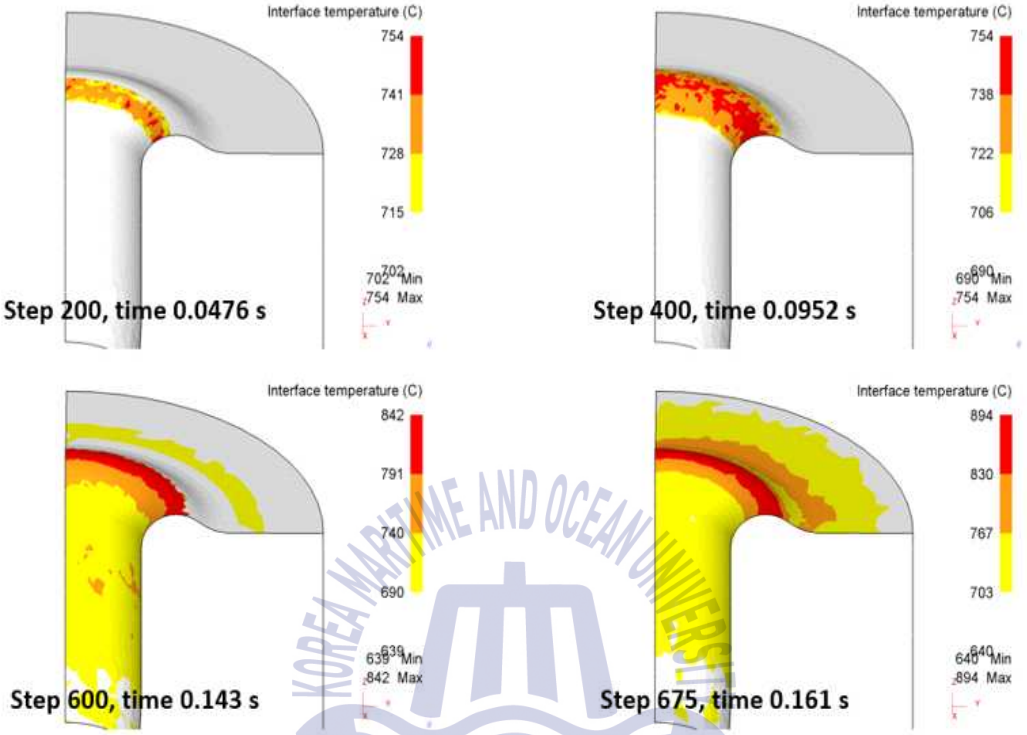

Fig. 3-8 Temperature distribution of conventional die

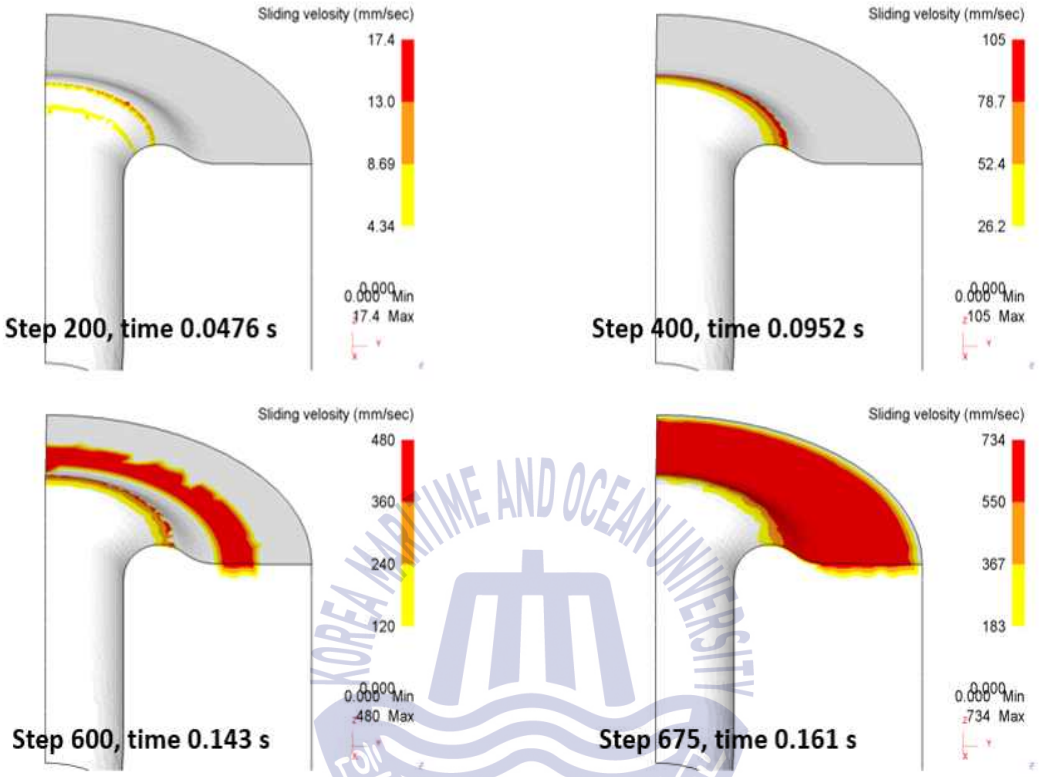

Fig. 3-9 Sliding velocity distribution of conventional die

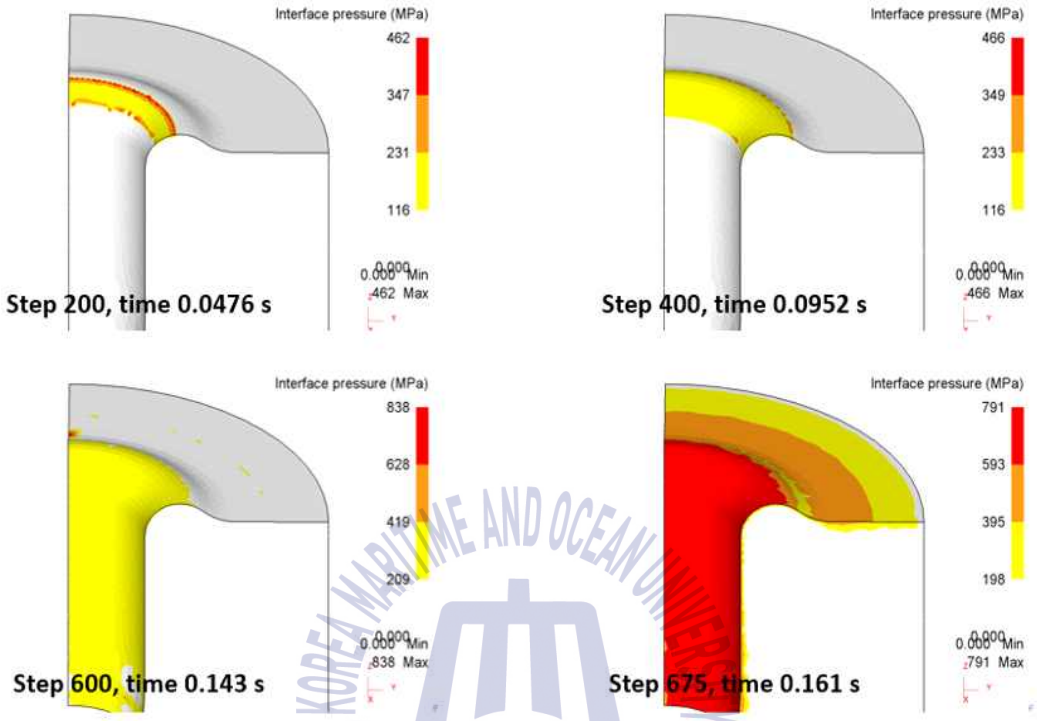

Fig. 3-10 Interface pressure distribution of conventional die

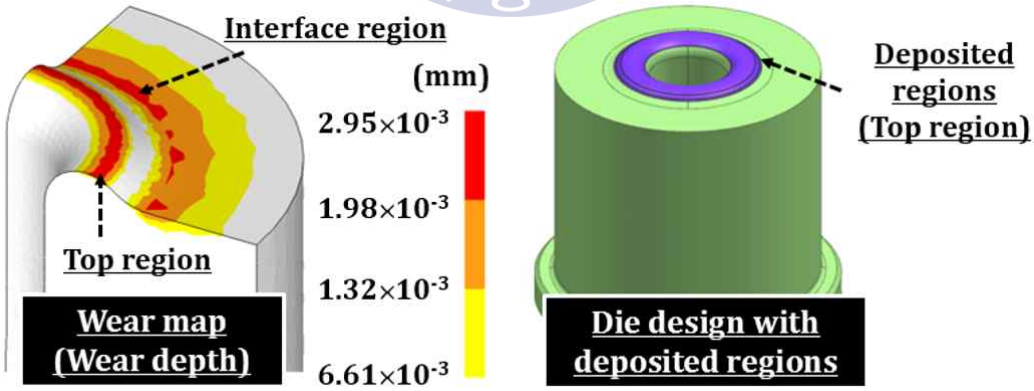

Fig. 3-11 Wear map of conventional die and die design with deposited regions

3.6.2 Simulation results of designed model

The wear speed of the mold has a direct relationship with the mechanical loading force. The greater the mechanical loading force, the greater the friction between the mold and the forged workpiece, and the faster the mold wears. Figure 3-12 shows the pressure-time curve of designed model during forging process. Compared with the traditional die forging process, it can be seen that the maximum mechanical loading force of the designed die in the forging process is smaller than that of the traditional die, which means that the designed die tool can cut down the surface friction and reduce wear.

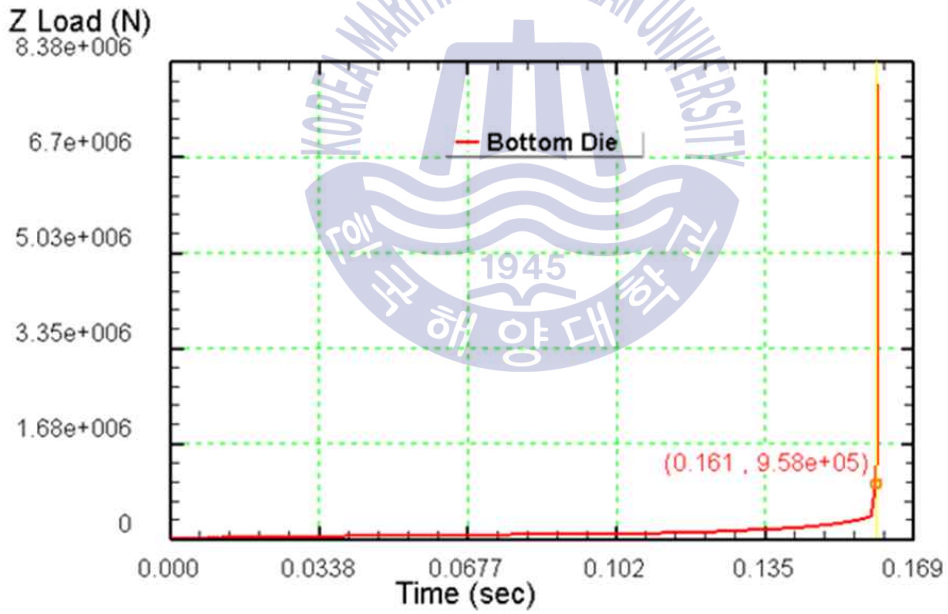

Fig. 3-12 Load-time curve of designed model during forging process

Figure (3-13) to (3-15) show the distribution of interface temperature, sliding velocity and interface pressure of automobile axle during forging process. According to Achard model, the wear of the model is directly related to the interface temperature, sliding velocity and interface pressure of the die. According to the simulation results, top region of the designed model is very easy to wear. Compared with the traditional molds, the designed die has the lower interface temperature, the faster sliping velocity and the smaller interface pressure, so the wear resistance of designed model is more excellent than traditional abrasive tools.

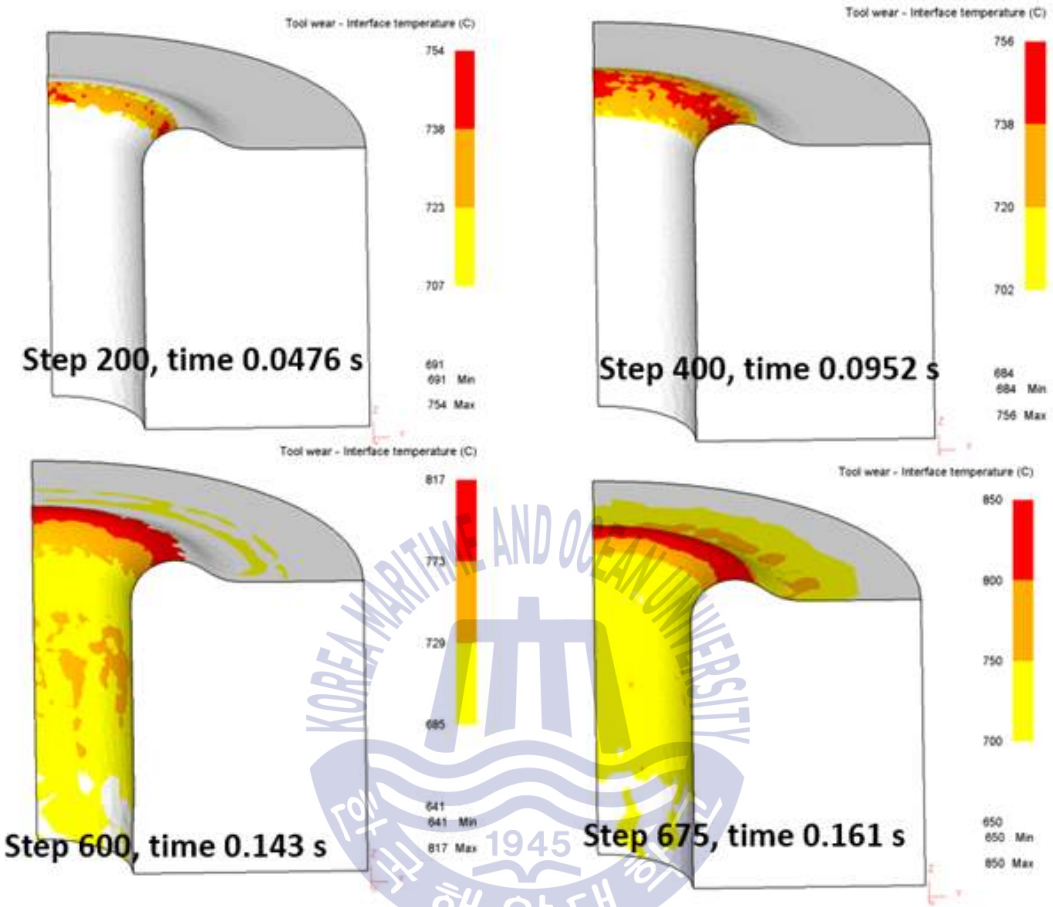

Fig. 3-13 Temperature distribution of designed die

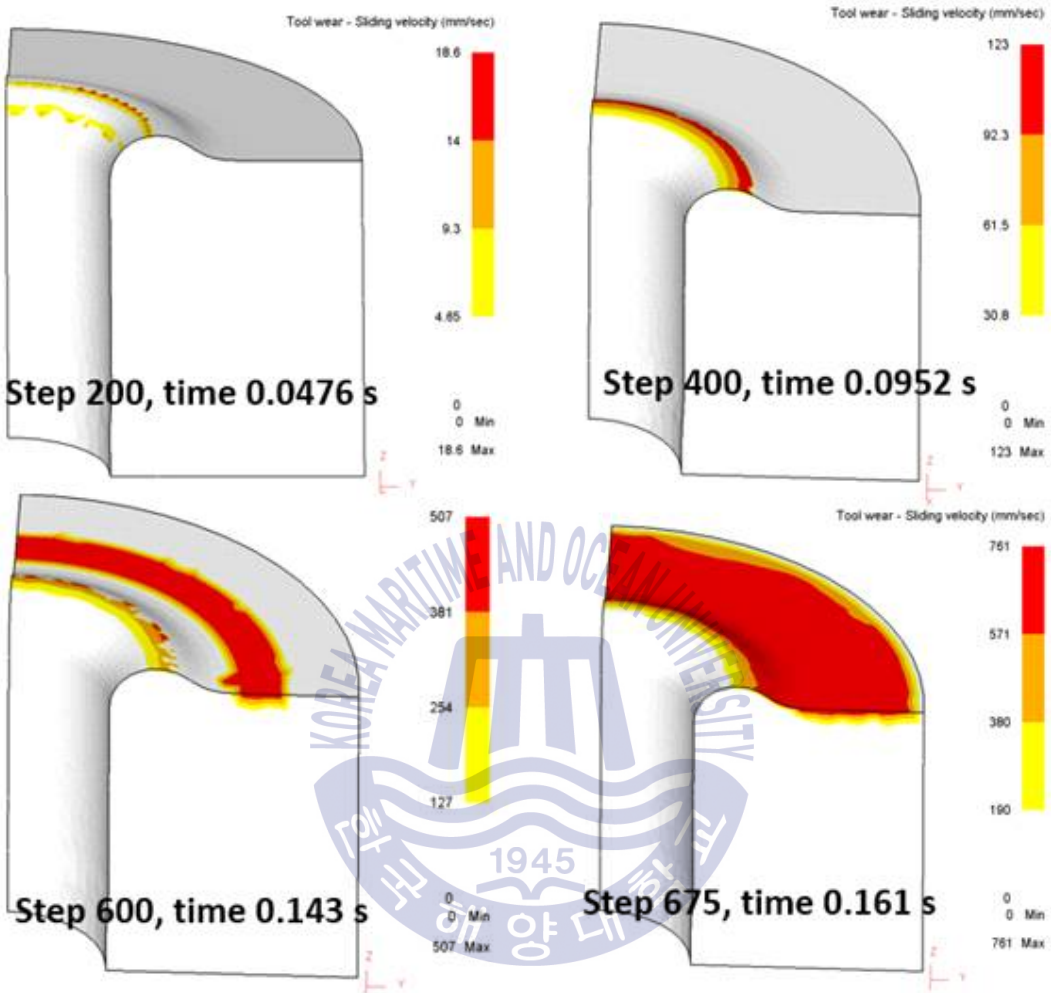

Fig. 3-14 Sliding velocity distribution of designed die

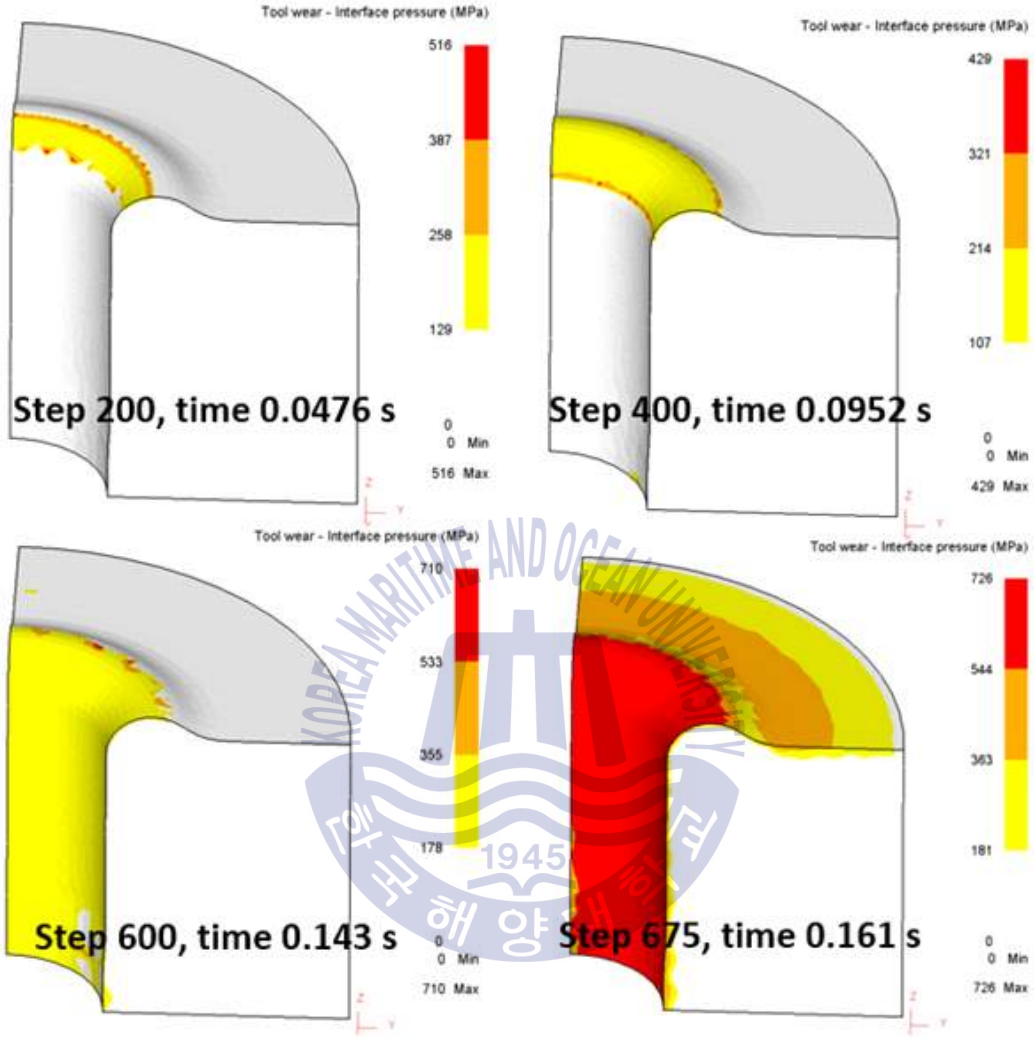

Fig. 3-15 Interface pressure distribution of designed die

Figure 3-16 shows the wear map of designed die. It can be seen from the figure, the most worn region appears at the top region of die surface. The maximum depth of wear is $5.99x10^{-5}$mm. Compared with traditional molds, the wear depth of designed dies is greatly reduced.

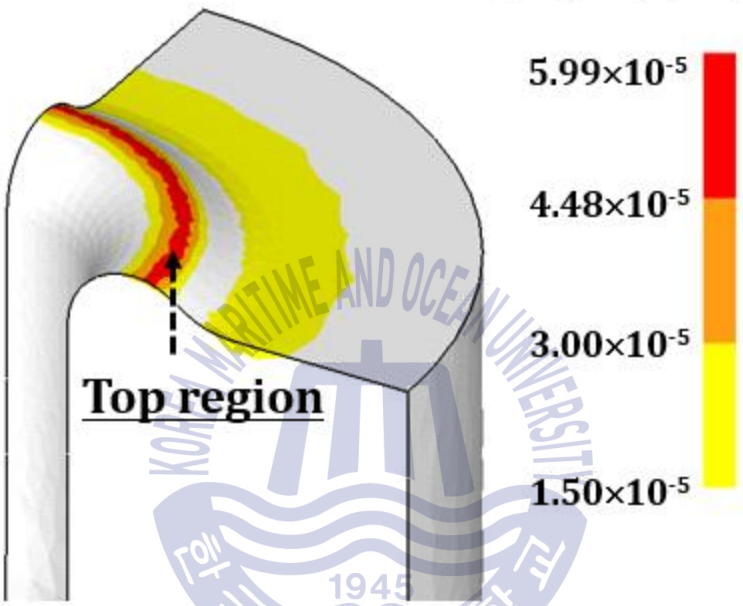

Fig. 3-16 Wear depth (mm) of designed die

3.6.3 Principal stress distribution on the conventional die and designed die

In the die forging process, the temperature of the die surface will increase due to heat conduction and mechanical friction, the temperature increase of die will cause thermal stress in deposited region, especially for the connection interface between the deposited layer and the substrate. Figure 3-17 shows the maximum principal stress distribution on the conventional die and designed die. It can be seen from the figure that there is a large stress difference between the deposited layer and the substrate of the designed mold, therefore, designed mold will generate a large thermal stress concentration

between the hardened layer and the substrate.

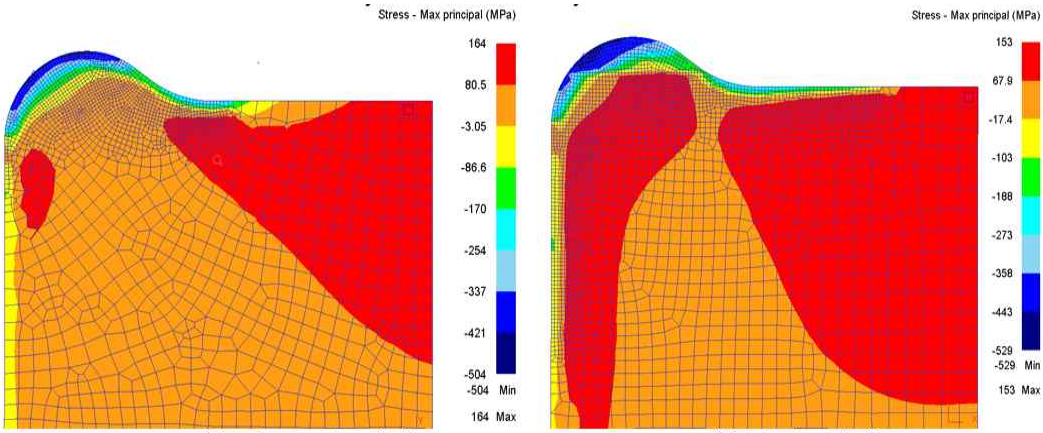

(a) Conventional die (b) Designed die

Fig. 3-17 Maximum principal stress distribution on the conventional die and designed die

Figure 3-18 shows the deviation of principal stress along the depositional interface. The orange dashed line represents the main stress difference along the depositional interface. The blue solid line represents the stress difference of the conventional mold at the same position as the depositional interface. By contrast, when Stellite21 is used for surface strengthening, a huge stress difference occurs between the deposited layer and the substrate, which is likely to cause cracks at the deposition interface. Therefore, in order to reduce the thermal stress difference at the depositional interface, we will design a optimal thermal stress control layers.

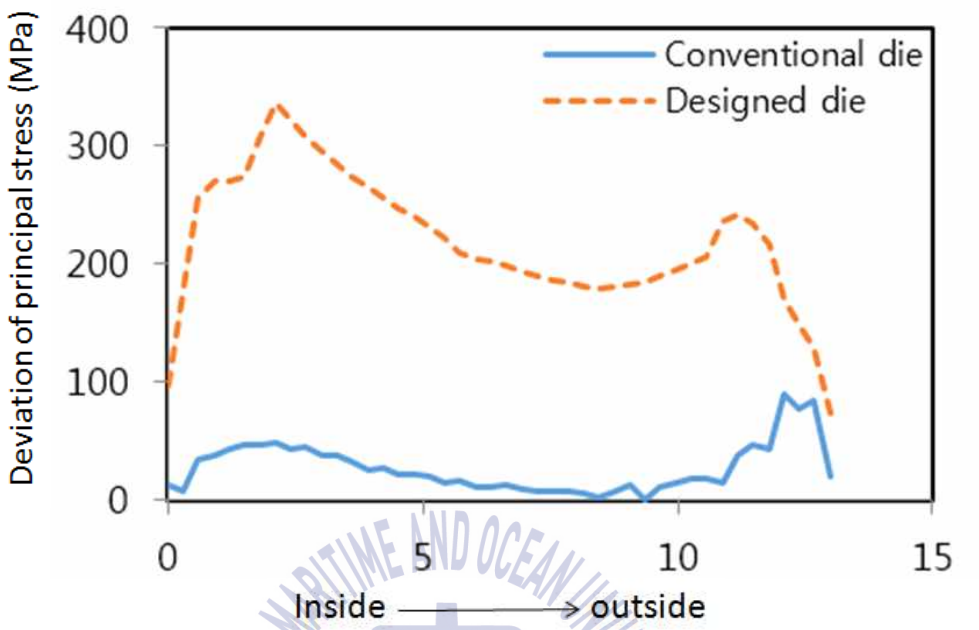

Fig. 3-18 Deviation of principal stress on the depositional interface

Chapter 4 Design of thermal stress control layers between hardened layer and substrate

In metal forming process, both plastic deformation and friction contribute to heat generation. Approximately 90 to 95% of mechanical energy involved in the process is transformed into heat[39]. A part of generated heat remains in the deformation material, another part flows into the undeformed or less-deformed portion of the material where temperature is lower, while still an additional part may flow into the tooling. The surface temperature of die will increase, thermal stress will generate at the interface of different materials. The size of the thermal stress has a direct impact on the service life of the abrasive. In this chapter, with the finite element simulation analysis method, the heat generation during deformation and heat transfer before, during and after deformation can be calculated in a computer, as well as thermal stress is calculated between the hardened layer and the substrate. A thermal stress control layers is designed between the hardened layer and the substrate to reduce the thermal stress, our aim is to minimize the thermal stress by changing the thickness and composition ratio of the transition layer.

4.1 Direct metal deposition technology

Due to heat transfer from the workpiece and heat generation by interface friction, the surface temperature of the bottom die rapidly increased. The wear is subjected to maximum pressure and sliding length under the highest temperatures, and therefore, the die are prone to wear leading to premature failure in the production process. The direct metal deposition technology, using laser 3D printing, is adopted to improve the wear resistance of the bottom die

surface at elevated temperatures.

The principle of the direct metal deposition technology is based the laser cladding process to create a hardfacing layer, it is almost the same as the laser cladding assisted hardfacing technology except for material deposition along the arbitrary trajectory through the layer-by-layer deposition in a CAD/CAM environment[40-43]. The dilution of the direct metal depostion technology is identical to the laser cladding assisted hardfacing technology. The thickness of a layer for the direct metal deposition technology ranges from 0.13 mm~0.38 mm[40]. The quality of the hardfaced layer by the direct metal deposition technology is dependent on the deposition direction, the laser power, the travel speed, the material feeding speed, the overlap ratio, the total layer thickness, the geometrical complexity, etc[44-48]. The direct metal deposition technology can control the bead width and thickness through optimization of the process parameters.

Figure 4-1 shows the direct metal deposition technology and deposited region on the bottom die. All materials are deposited by laser cladding. The laser process utilizes gas-atomised powder that, with the assistance of a laser beam, is locally melted onto a substrate material in a controlled atmosphere. To create a metallically bonded clad layer the substrate is melted to a depth about 50um. The shallow melt depth and the efficient cooling provided by the substrate material combine to create a clad layer with desired composition and a fine microstructure[32]. Multiple clad layers can be deposited. Comprehensive research has been performed in the area of laser cladding of stellites[49-54].

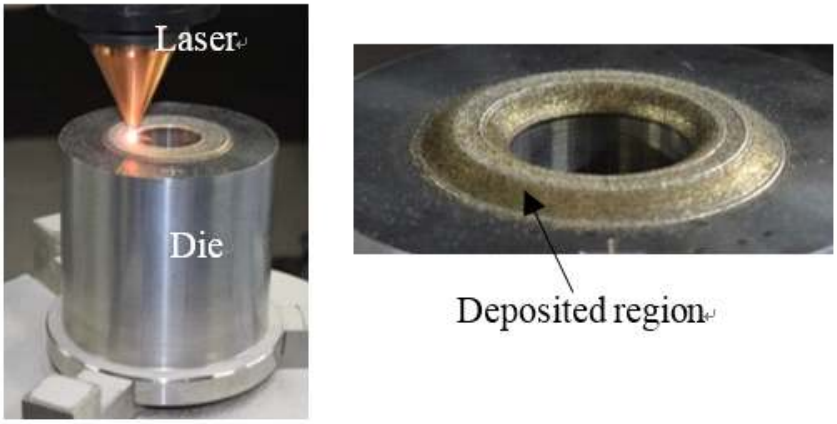

Fig. 4-1 Deposition process and deposited region of bottom die

4.2 Design of thermal stress control layers

SKD61 as substrate material is applied to the bottom die, and the hardfacing layer is made of Stellite21. Table 3-1 shows the main chemical composition of Stellite21 and SKD61. Their chemical composition and physical properties have a large deviation, particularly their thermal physical properties; therefore, thermal stress concentration appears near deposition interface between the hardfacing layer and the base metal after hot forging.

In order to reduce thermal stress, TSCL is designed between the hardfacing layer and the base metal. Figure 4-2(a) illustrates the deposited layer structure of the hardfacing layer, TSCL, and substrate. The thickness of deposited region is about 3 mm. Figure 4-2(b) exhibits the designed geometric shape and thickness of the TSCL. The thicknesses of the TSCL are 1 mm, 1.5 mm, and 2 mm respectively. A mixture of SKD61 and Stellite21 is selected as the material of TSCL. Mixing ratios (volume) of Stellite21 are set as 25%, 50%, and 75%. Several cases are shown in Table 4-2.

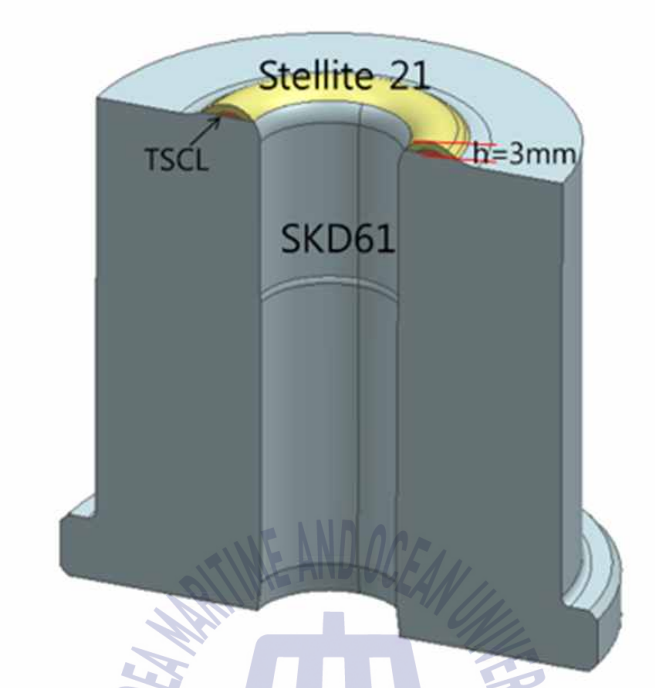

(a) Axle die and deposited region

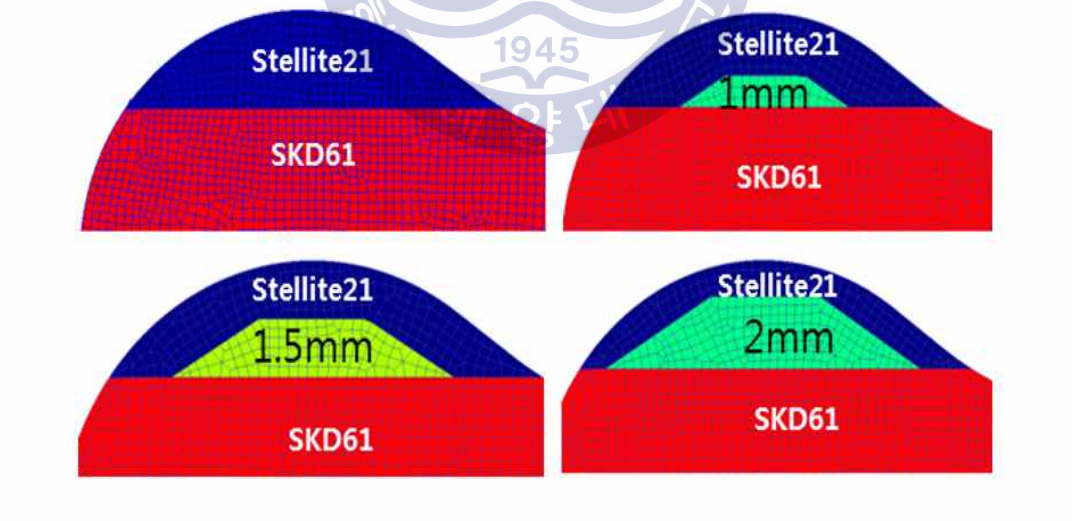

(b) Design of TSCL

Fig. 4-2 Axle die and geometry model of TSCL

Table 4-1 Thickness and mixing ratio of TSCL

Case	Thickness of TSCL (mm)	Volume ratio of Stellite 21(Φ)
Reference case	0	——
Case 1	1	0.25
Case 2		0.5
Case 3		0.75
Case 4	1.5	0.25
Case 5		0.5
Case 6		0.75
Case 7	2	0.25
Case 8		0.5
Case 9		0.75

4.3 Numerical analysis of axle forging process

The thermal and physical properties of SKD61 and Stellite21 are shown in Figure 4-3. The property data of the Stellite 21 alloy and SKD61 are obtained from the related references. There is lack of data regarding the properties at high temperature, and therefore, these data are assumed by the line interpolation method in the analysis.

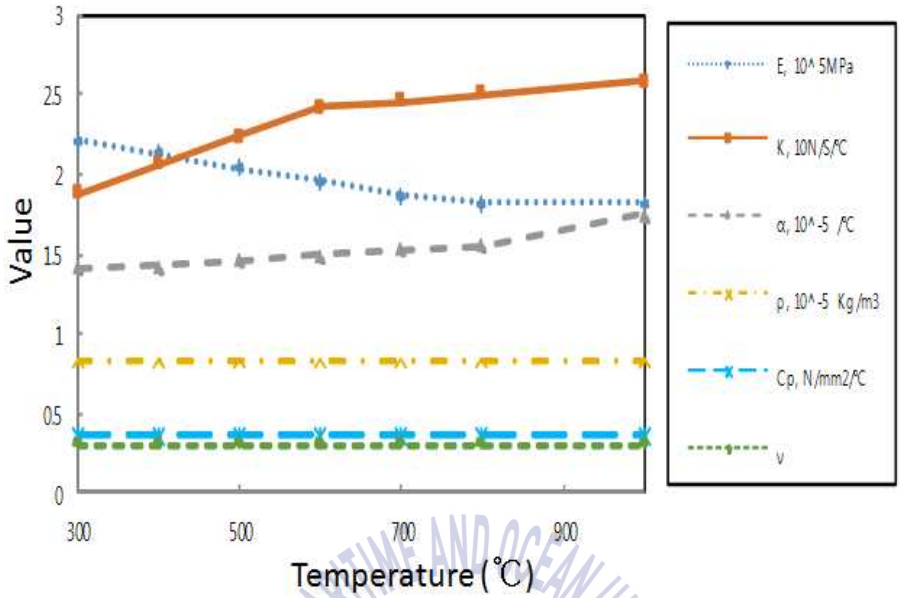

(a) Stellite 21

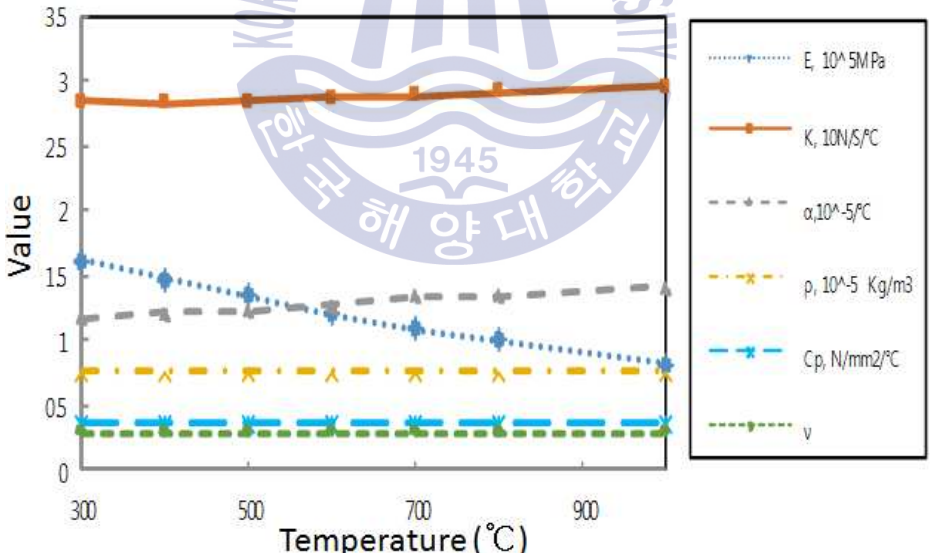

(b) SKD61

Fig. 4-3 Thermal and physical properties of Stellite21 and SKD61

The TSCL is the mixture of SKD61 and Stellite 21, and different mixing ratios of SKD61 and Stellite 21 will engender different performances. In this study, the mixing law[55] and Maxwell model[56] are generally used to describe the physical properties of the TSCL. The relation equations are as shown below:

$$\xi_{TSCL} = \xi_1(1-\Phi) + \xi_2\Phi \tag{40}$$

$$C_{PTSCL} = \frac{\rho_1 C_{P1}(1-\Phi) + \rho_2 C_{P2}\Phi}{\rho_1(1-\Phi) + \rho_2\Phi} \tag{41}$$

$$\frac{K_{TSCL}}{K_1} = \frac{K_2 + 2K_1 + 2\Phi(K_2 - K_1)}{K_2 + 2K_1 - \Phi(K_2 - K_1)} \tag{42}$$

where ξ_{TSCL} is the thermal physical properties of TSCL, ξ_1, ξ_2 are the thermal physical properties of SKD61 and Stellite21. Φ is the volume of Stellite21. C_{PTSCL} is the specific heat of TSCL, C_{P1}, C_{P2} are the specific heat of SKD61 and Stellite21. ρ_1, ρ_2 are the density of SKD61 and Stellite21. K_{TSCL} is the thermal conductivity of TSCL, K_1, K_2 are the thermal conductivity of SKD61 and Stellite21. Thermal physical properties of TSCL is shown in Table 4-2.

Table 4-2 Thermal physical properties of TSCL

Properties	TSCL mixing ratio Φ - 0.25		TSCL mixing ratio Φ - 0.5		TSCL mixing ratio Φ - 0.75	
	Temp [℃]	Value	Temp [℃]	Value	Temp [℃]	Value
Young's modulus [GPa]	25	211.3	25	222.5	25	233.8
	649	133.3	649	152.8	649	172.2
	760	123.3	760	143.1	760	162.6
Thermal expansion [10^{-6}mm/mm · ℃]	100	11.05	100	11.7	100	12.4
	425	12.73	425	13.25	425	13.8
	650	13.6	650	14.1	650	14.6
Thermal conductivity [W/m^2 · ℃]	200	25.7	200	22.9	200	20
	400	26.6	400	24.64	400	22.65
	600	27.64	600	26.53	600	25.38
Specific heat [J/kg · ℃]	450.2		440.8		431.8	
Density [kg/m^3]	7903		8045		8188	
Poisson's ratio	0.29		0.3		0.3	

The axle manufacturing process is complicated, since the bottom die is subjected to constantly changing pressure and temperature. Figure 4-4 is description of a single forging cycle of the axle. One single forging cycle takes about 16 s.

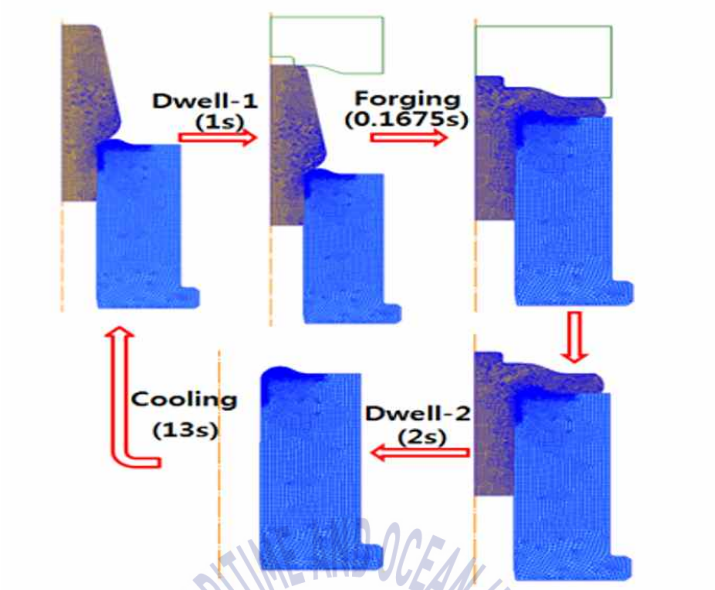

Fig. 4-4 Description of a single forging cycle

4.4 Simulation results and discussion

4.4.1 Die temperatures during steady-state

Temperature is the main cause of thermal stress; hence, accurate stress analysis requires the investigation of the production process under steady-state conditions. All forming processes, especially warm/hot forging, have a transient warm-up period before the dies reach their steady operating temperature distribution. Most FE simulation analyses ignore this warm-up stage by assuming a certain preheat temperature for the die, which is acceptable for metal flow analysis.

Figure 4-5 shows a schematic of the warm-up phase of the hot forging die of axle with an initial preheat temperature of T_0(350℃). The die temperature increases until a steady-state cycle is reached, as shown in Figure 4-5. The solid line represents the fluctuation amplitude of the surface temperature of the bottom die, while the dotted line represents the fluctuation amplitude of

the temperature at the center point of the TSCL. The steady-state temperature (Ti) is reached after 14 cycles.

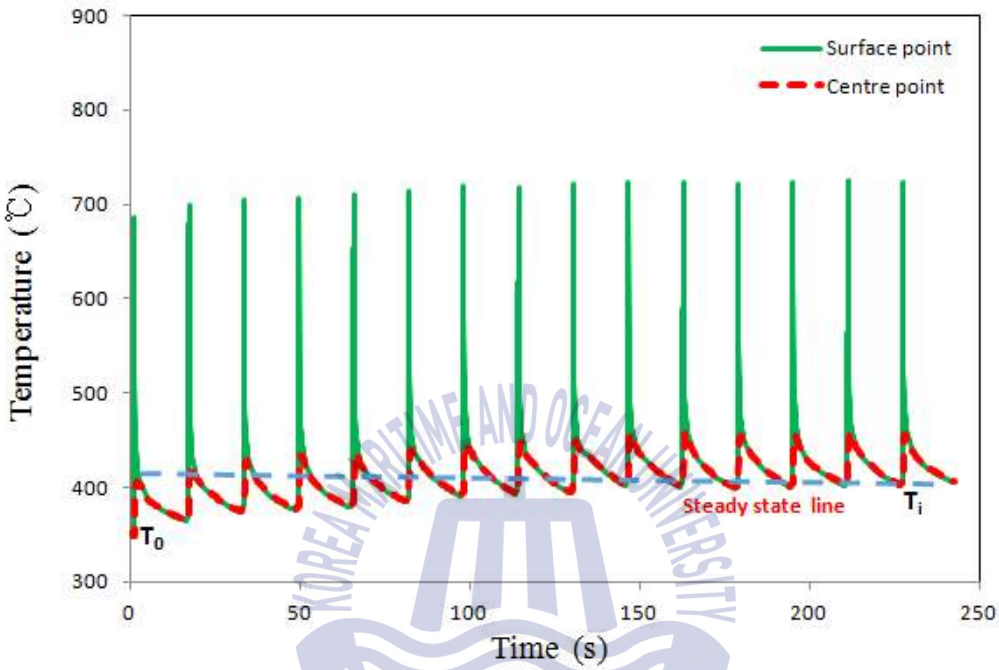

Fig. 4-5 Temperature change of warm-up in forging dies

In order to simulate the true stress distribution in the deposited region during the work state, the forging state and cooling state of the bottom die are analyzed in the 14th cycle.

4.4.2 Die state under steady state conditions

4.4.2.1 Stress distribution on the deposited layer at forging state

During the forging process, heat transfer and frictional heat generation between the workpiece and dies result in an increase of localized temperature. As shown in Figure 4-2, the Stellite 21 alloy has a lower heat capacity, faster heat transfer speed, and greater expansion coefficient than

SKD61. Therefore, when the localized temperature of the die increases, the surface of Stellite21 rapidly expands, and a stress concentration region, which provides a favorable condition for the formation of thermal cracks, occurs between the deposited layer and the base metal.

Figure 4-6 displays the maximum principal stress distribution of all cases at the end of the process under steady state conditions, in which the bottom die bore maximum load and stress. According to the maximum principal stress distribution in the figure, there is a large deviation of maximum principal stress near the intersection line between the hardfacing layer and the substrate of reference case. When a TSCL, consisting of Stellite21 and SKD61 is created between the hardfacing layer and the substrate to release thermal stress, the maximum principal stress changes from the original dislocation transition to the smooth transition at the deposited interface. Thus, stress concentration is reduced near the intersection line.According to the comparison of the thickness and composition change of the TSCL, when the ratio of Stellite21 is increased and the thickness of TSCL is kept constant, the red region shown in Figure 4-6 (tensile stress region) is reduced. This shows that the gradient of principal stress increases at the interface between the TSCL and the base metal, while the gradient of principal stress decreases at the interface between the TSCL and the hardfacing layer. When the thickness of TSCL is increased and the ratio of Stellite21 is remained, the blue region shown in Figure 4-6 (compressive stress region) increase and red region will decrease. As a consequence, the middle region is gradually increasing, meaning that the gradient of the intermediate transition zone is relatively gentle; the gradient of principal stress between the TSCL and the hard facing layer is gradually reduced.

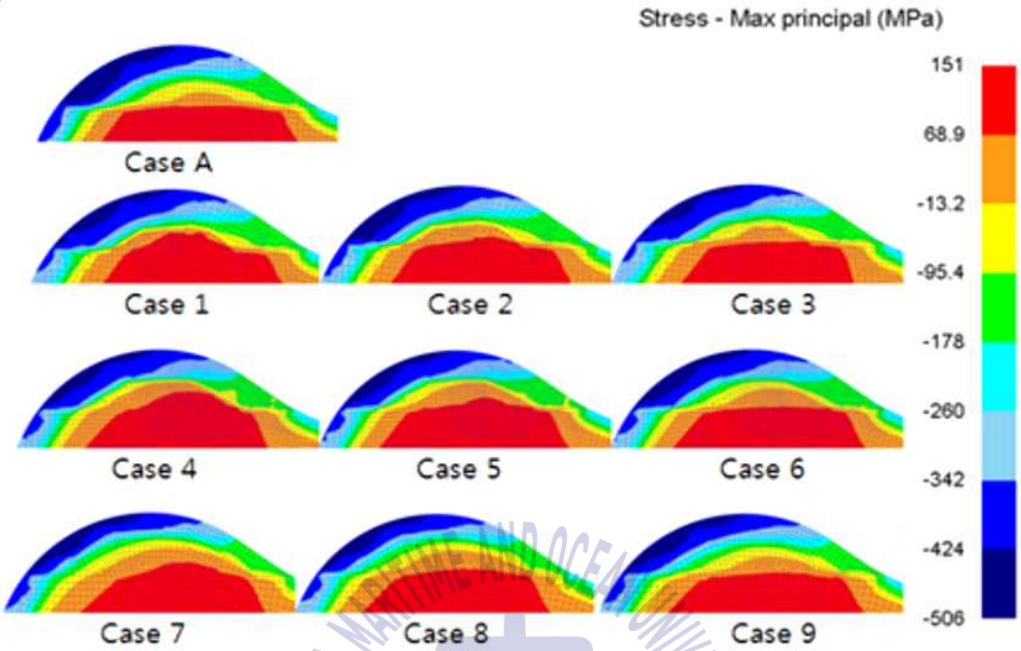

Fig. 4-6 Max principal stress distribution in the deposited region under the maximum loading

In order to clearly compare the effect of different thicknesses and compositions of a TSCL on the interface, the deviations of maximum principal stress on both sides of the interface are studied. Figure 4-7 shows the main interface of stress concentration after adding the TSCL. The magnitude of the stress concentration will vary with the composition and thickness of the TSCL on both interfaces A and B.

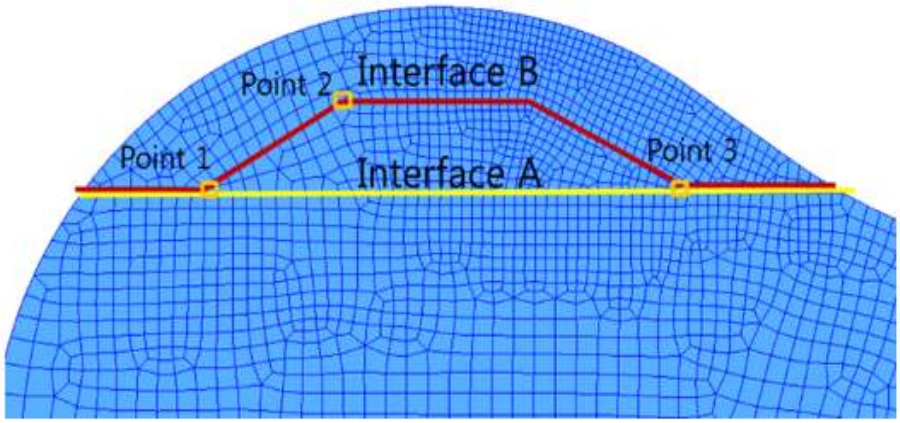

Fig. 4-7 Main interface of stress concentration

Figure 4-8 displays the deviation of maximum principal stress along interfaces A and B. All cases with a TSCL are compared with reference case. Figure 4-8 shows the results of all relevant comparisons along interface A. It is shown that all cases with a TSCL produce better results than reference case on interface A. In other words, when a TSCL is created, stress concentration is reduced on interface A. However, when the thickness of TSCL is 1 mm, only the section with the TSCL added shows a lower deviation of principal stress as compared to reference case; while the interface directly connected the hardfacing layer and the base metal shows either equal or slightly higher deviation values as compared to reference case (as shown in Figure 4-8 (a)). Hence, when the TSCL is set as 1 mm, it plays a very small role in reducing interfacial thermal stresses. When the thickness of the TSCL increases, the deviation of principal stress on interface A is reduced. The deviation of principal stress on interface A is the smallest when the thickness of the TSCL is 2 mm. Apart from that, it is known that if the thickness of TSCL is kept constant, as the volume fraction of Stellite21 alloy is increased, the deviation of principal stress at the interface between TSCL and the base

metal is increased.

Figure 4-8 (d), (e), and (f) show the results of all cases with a TSCL along interface B. According to the results, the deviation of principal stress at the interface between TSCL and the hardfacing layer will increase when content of Stellite21 is decreased in the TSCL. When the volume fraction of Stellite 21 is 25%, the deviations of principal stress values on interface B are generally higher than in reference case. Therefore, Case 1, Case 4, and Case 7 are more apt to form thermal cracks on interface B. Considering interface A and B, only Cases 5, 6, 8, and 9 are relatively better. The deviation of principal stress of Case 6 is smaller than Case 5 on the interface B, but it is greater on interface A and its peak value is higher than in Case 5 (as shown in Figure 4-8 (e)). The same goes when comparing Cases 8 and 9, meaning Case 8 produced better results than Case 9.

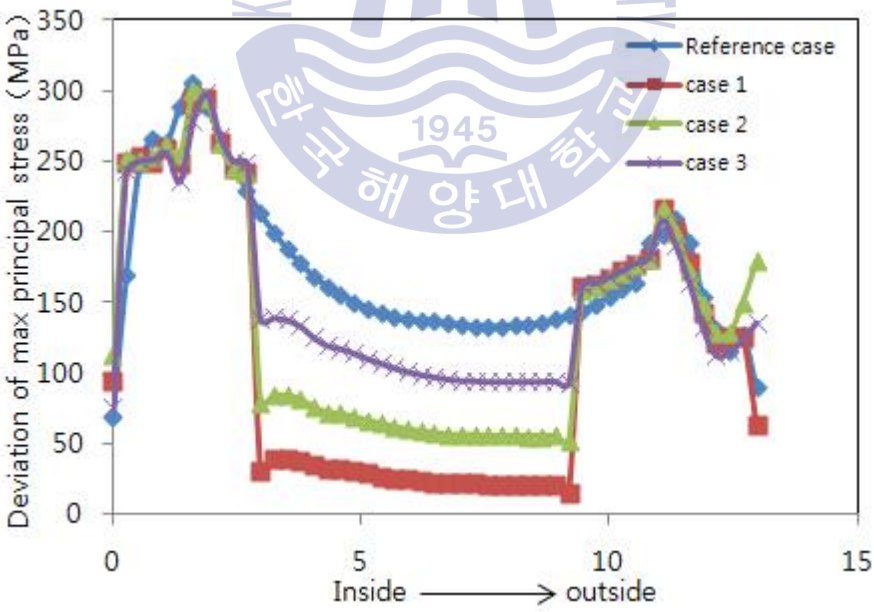

(a) Interface A-TSCL (1 mm)

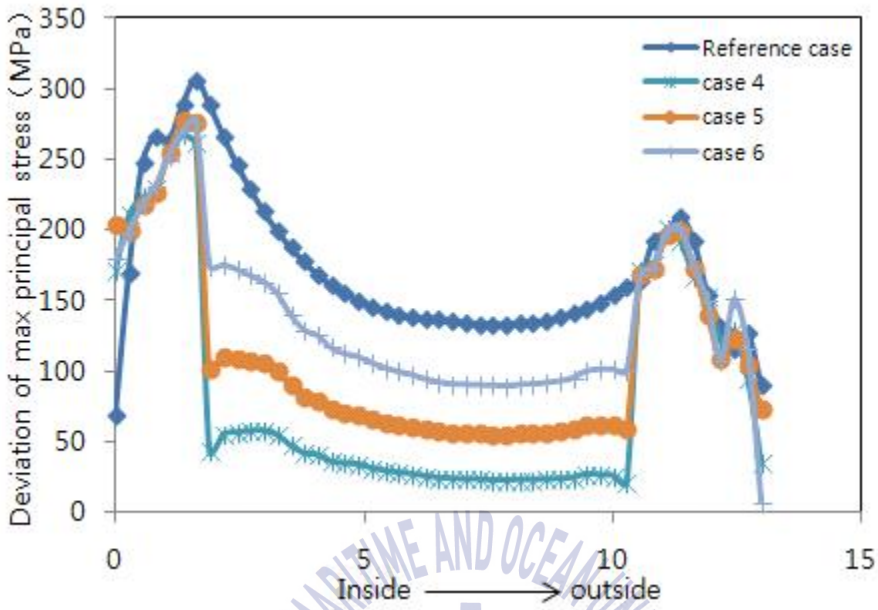

(b) Interface A-TSCL (1.5 mm)

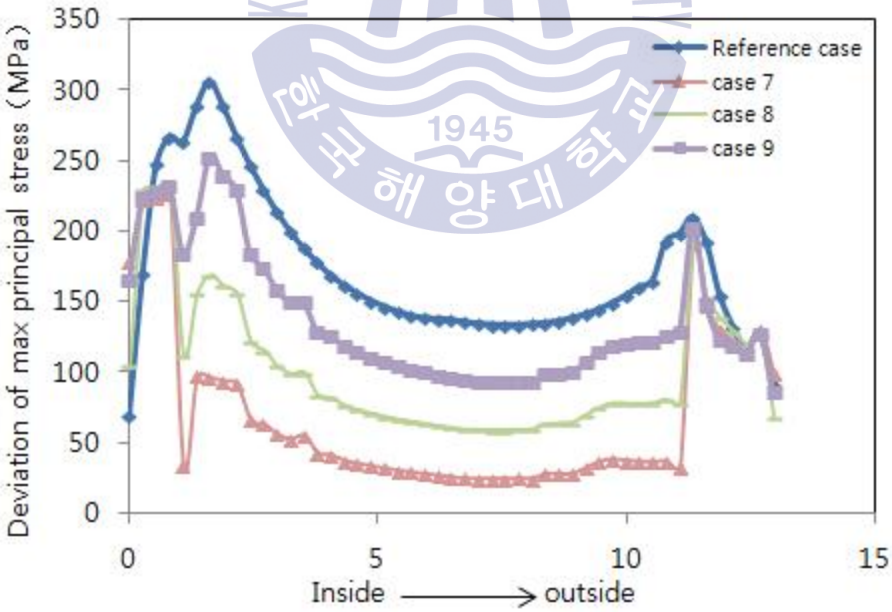

(c) Interface A-TSCL (2 mm)

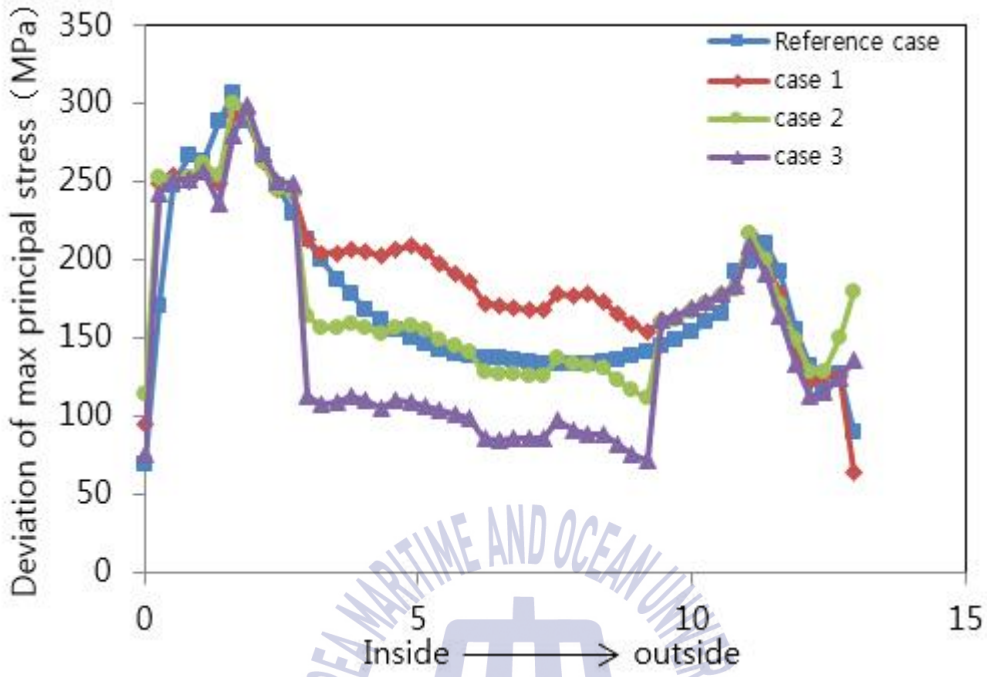

(d) Interface B-TSCL (1 mm)

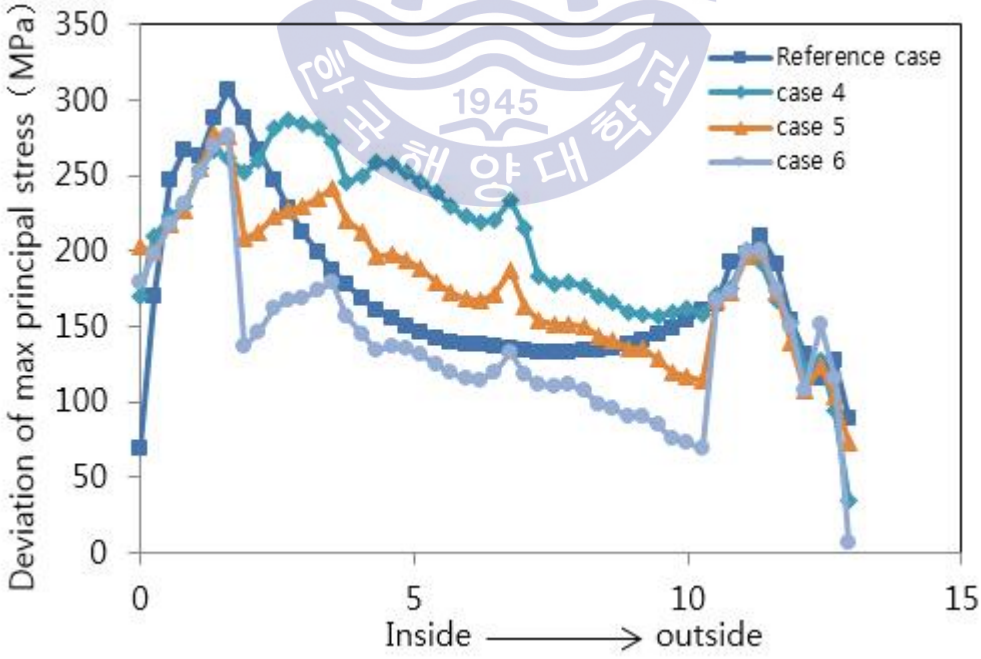

(e) Interface B-TSCL (1.5 mm)

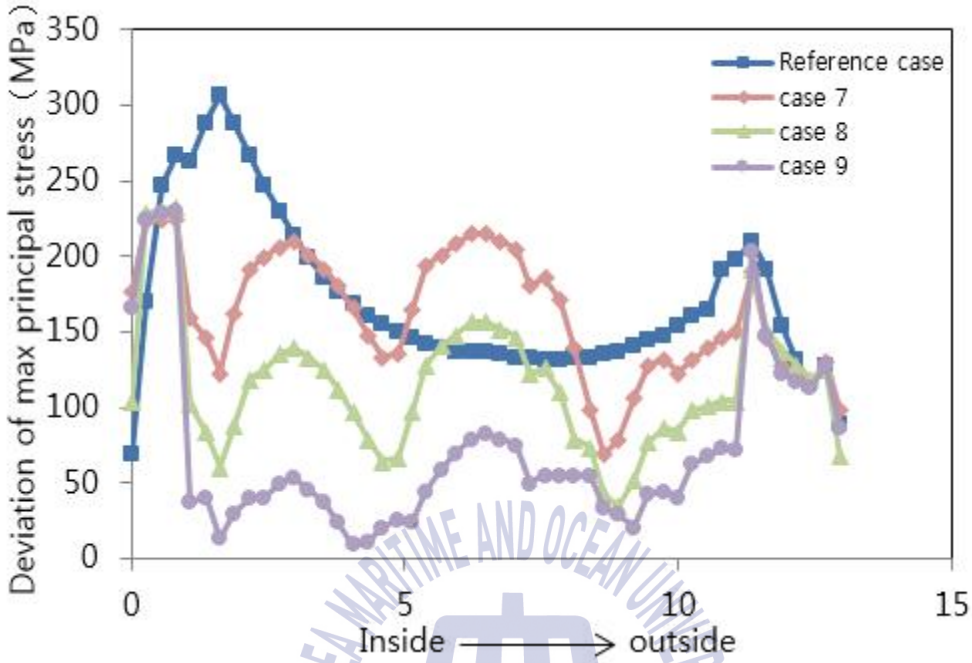

(f) Interface B-TSCL (2 mm)

Fig. 4-8 Deviation of max principal stress along interface A and interface B at the forging state

4.4.2.2 Deviation of die strain at the interface

Localized heating can form a greater temperature gradient in the deposited region. The closer the surface of the bottom die, the bigger the temperature gradient. At high temperatures, the elastic modules of deposited material decrease and strain is more likely to occur under the same stress. Figure 4-9 shows the forging temperature distribution on the bottom die. The red loop represents the boundary of the TSCL. We can clearly see that when the thickness of TSCL is 2 mm, the boundary of the TSCL lies in local high temperature zones, and the difference of the external and internal temperatures is relatively large on the interface. Therefore, a large the

deviation of strain will appear, which may lead to the formation of fatigue cracks.

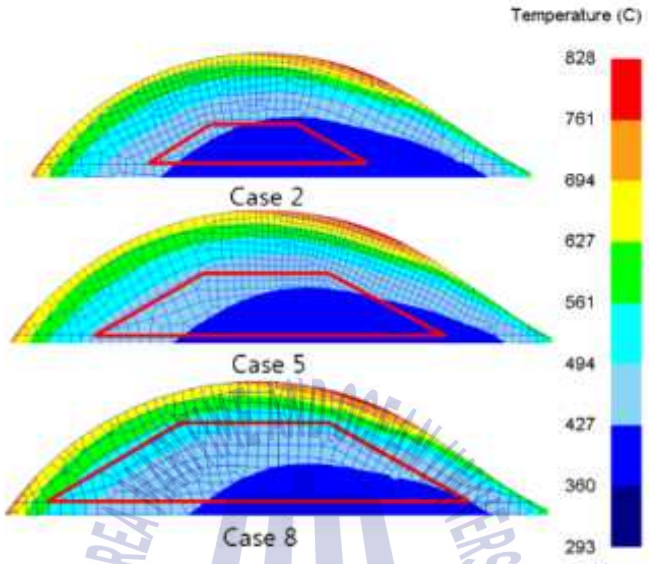

Fig. 4-9 Temperature distribution on the deposited layer of bottom die

Figure 4-10 shows the deviation of maximum principal strain at points 1-1 (between the hardfacing layer and the base metal), 1-2 (between the TSCL and the base metal), 1-3 (between TSCL and hardfacing layer), as well as point 2 and point 3 (between the hardfacing layer and the base metal) (as shown in Figure 4-7). The results show that the largest deviation of principal strain at the interface occurs when the thickness of the TSCL is 2 mm. Therefore, cases where the thickness of the TSCL is 2 mm are unsafe.

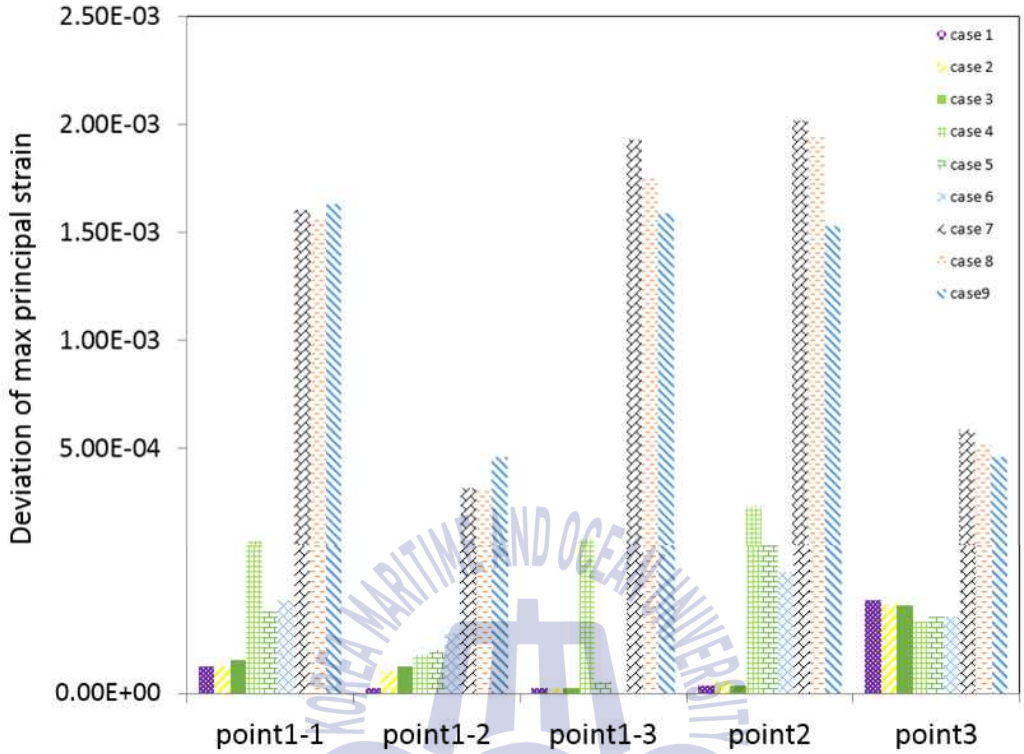

Fig. 4-10 Deviation of max principal strain at forging state

Based on the above analysis, when the thickness of the TSCL is 1 mm, the TSCL plays only a minor role in relieving stress. When the thickness of TSCL is 2 mm, the interface is affected by temperature and a greater strain is produced. Therefore, the optimal thickness of the TSCL is 1.5 mm and the optimal mixing ratio is for the content of Stellite21 is 50% according to the stress analysis on the interface at the forging state.

4.4.3 Residual stresses on the die after cooling stage

After cooling, the pressure is removed, and only residual stress remains on the bottom die. Residual stress is an important factor of material cracking, and controlling residual stress can effectively reduce the formation of cracks. After forging, the high temperature workpiece removed from the bottom die

and the temperature of the die begins to decrease. Before forging the next workpiece, the temperature of the die must be decreased to a minimum value. At this moment, a deviation of residual stresses would be expected in the deposited region. Figure 4-11 displays the maximum principal stress distribution in the deposited region after cooling. reference case without a TSCL forms a large deviation of max principal stress between the deposited layer and the base metal, and the largest deviation of maximum principal stress appears at the center of the deposited region. When the TSCL is applied, the residual stress between the TSCL and the base metal is greatly reduced as the thickness of the TSCL increases. In particular, when the thickness of TSCL is increased to 2 mm, the residual stress will be lower than 70 MPa. The maximum deviation of maximum principle stress appears at the three-phase interface after the TSCL is added. When the Stellite21 content is increased while maintaining the thickness of TSCL, the deviation of max principal stress increases on interface A and decreases on interface B.

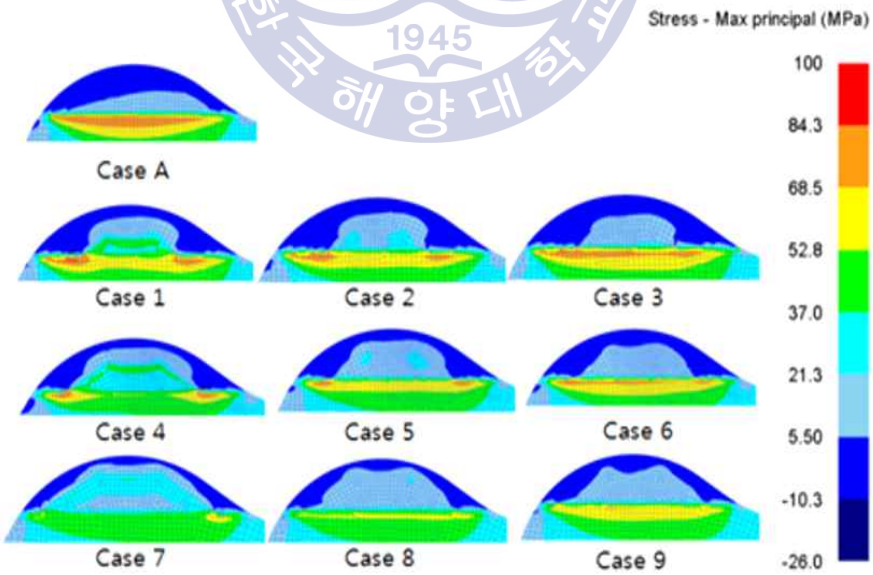

Fig. 4-11 Maximum principal stress distribution in the deposited region at the cooling state

Figure 4-12 shows the deviation of maximum principal stress distribution on interfaces A and B. Figure 4-12 (a), (b) and (c) show the result of all cases with a TSCL being compared with reference case along interface A. Figure 4-12 (d), (e) and (f) show the results of all cases with a TSCL being compared with reference case along interface B. According to the results, when a TSCL is applied, residual stress is mainly concentrated on the interface without a TSCL. When the proportion of Stellite21 is 25%, the deviation of maximum principal stress is relatively small on interface A, but relatively large on interface B and the maximum deviation is very high. As a result, thermal cracks may be formed in advanceat the three junctions and extended along interface B. When the proportions of Stellite21 are 50% and 75% respectively, their maximum deviation values are mostly equal with reference case and the deviation of maximum principal stress is relatively small. However, when the proportion of Stellite 21 in the TSCL is 50%, the deviation of max principal stress at the interface with a TSCL on interface A is lower in comparison to a Stellite21 proportion in the TSCL of 75%. However, they are almost equal on interface B. Therefore, we concluded that the optimal mixing ratio for the TSCL is a 50% proportion of Stellite21 at the cooling state.

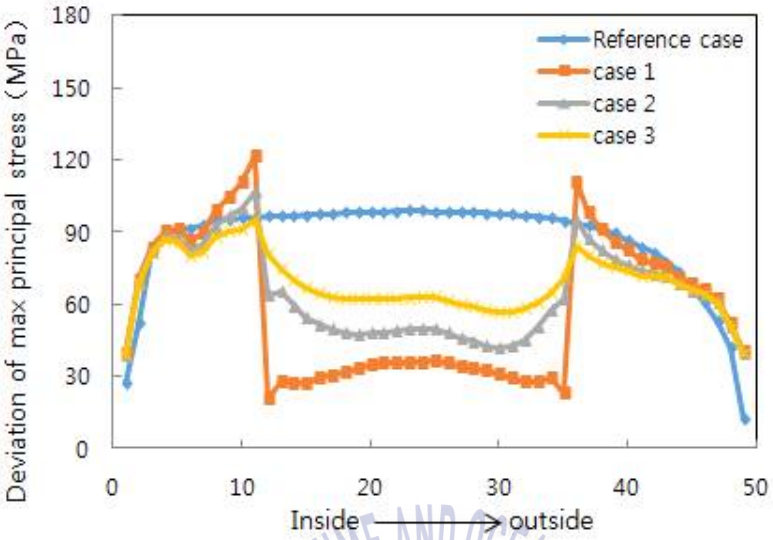

(a) Interface A-TSCL (1 mm)

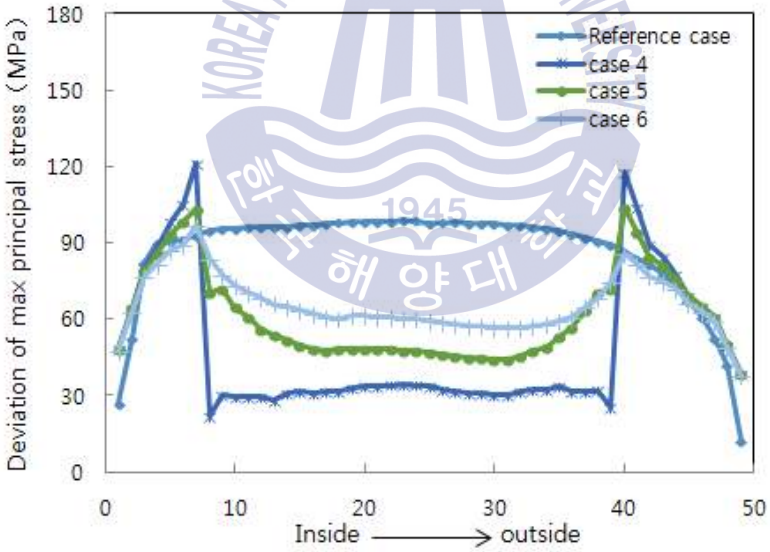

(b) Interface A-TSCL (1.5 mm)

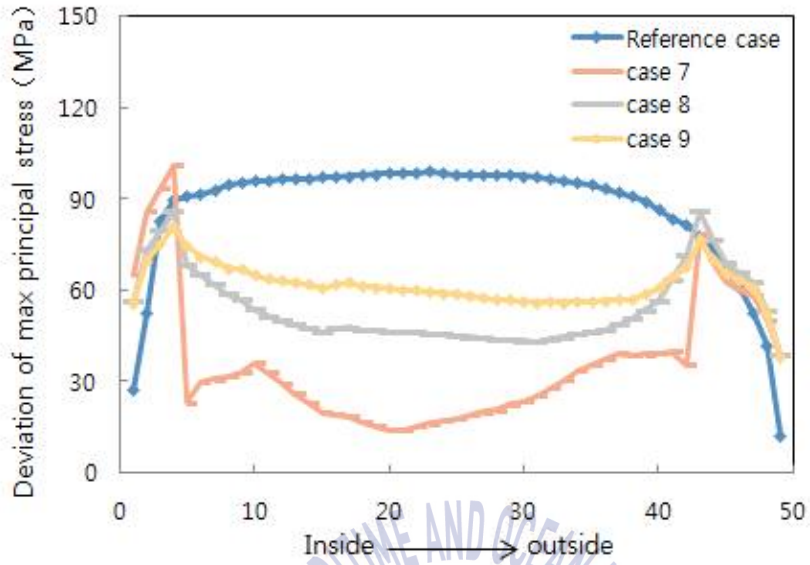

(c) Interface A-TSCL (2 mm)

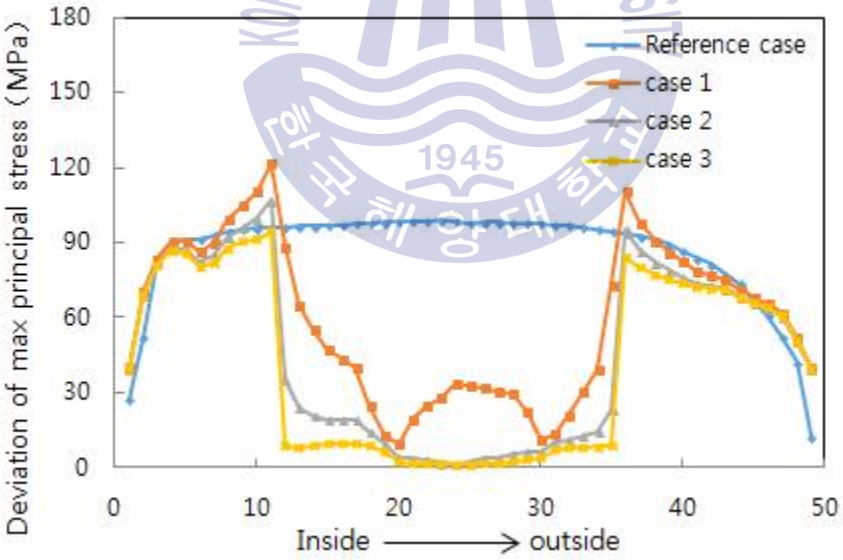

(d) Interface B-TSCL (1.5 mm)

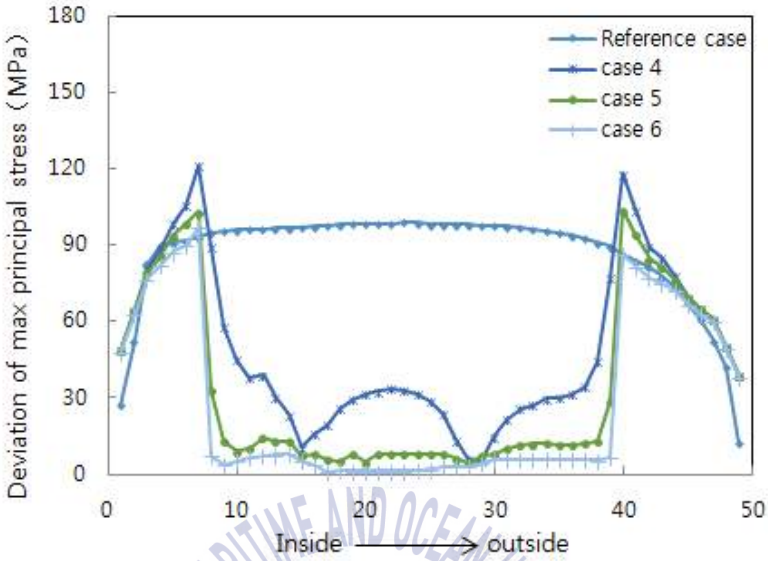

(e) Interface B-TSCL (1.5 mm)

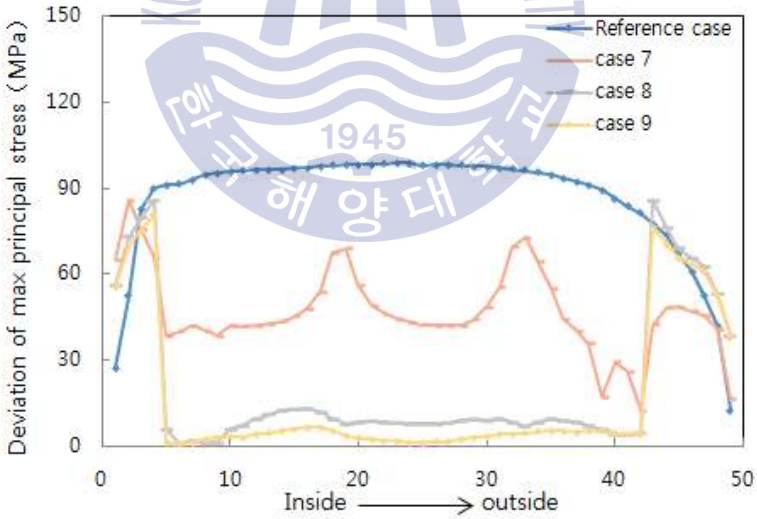

(f) Interface B-TSCL (2 mm)

Fig. 4-12 Deviation of maximum principal stress along interface A and interface B at the cooling state

Chapter 5 Microstructure and hardness of Stellite21 deposited on the hot forging die

Die life acts as an important factor on the steel parts productivity, it directly affects the cost of steel workpiece. Extending the service life of the abrasive tool is an effective way to reduce the cost of the workpiece. Therefore, direct metal rapid tooling assisted hardfacing technology is developed and applied. The hardfacing technology is to increase the service life of the grinding tool by increasing the strength and wear resistance of the surface of the grinding tool. A laser is generally used as an auxiliary heat source to weld an excellent material to the surface of the grinding tool. The choice of alloy is particularly important, alloys used at elevated temperature require two main characteristics: first, adequate resistance to corrosive attack and, secondly, sufficient mechanical strength to resist deformation or fracture under the imposed stresses. Cobalt base alloy is often employed on account of the good resistance to thermal fatigue and the good hardness at elevated temperature.

In this chapter, a cobalt base coating (Stellite21) is deposited using a locally selective deposition technology on a low alloyed steel. Thermomechanical behavior and microstructure of Stellite21 alloy are researched after the effects of heat and stress, the results show the material parameters related to the microstructural evolution of the cobalt superalloy during the tests.

5.1 Cobalt alloy

Cobalt-base alloys can be conveniently categorized as follows:

- High-carbon alloys designed for wear service
- Low-carbon alloys designed for high-temperature service

- Low-carbon alloys designed to combat corrosion or simultaneous corrosion and wear

Many of the properties of the alloys arise from the crystallographic nature of cobalt, Co (in particular its response to stress), the solid solution strengthening are relative to the content of chromium, Cr, tungsten, W, and molybdenum, Mo, and the formation of metal carbides,

The strengthening of cobalt base alloy is provided by solid solution strengthening of the matrix and by the precipitation of carbides. Solid solution strengthening is principally due to the contents of addition elements, such as chromium, nickel, molybdenum, tungsten etc. The second-phase strengthening in cobalt base alloy is mainly provided by carbides formed from the chromium, which is primarily provide corrosion resistance.

Stellite21 is a cobalt-based superalloy with chromium (Cr), molybdenum (Mo), and carbon (C) as major alloy elements. Compared with other Stellite alloys, Stellite21 contains considerably less carbon (0.25 wt%) so that it is strengthened not only by carbides but also a solid solution with the strengthening effect imparted mainly by Mo[57]. Also by virtue of the high Mo content, and the fact that most of the Cr is in the solid solution (rather than in Cr_7C_3 carbides), the alloy is more resistant to corrosion than other Stellite alloys. Stellite21 has several unique properties, such as creep-resistance and mechanical strength at elevated temperatures, resistance to wear, bio-compatibility, and corrosion resistance to body fluids. Stellite21 contains low carbon content so that its hardness and wear resistance are relatively low compared with other wear-resistant Stellite alloys. If its hardness and wear resistance are improved, Stellite21 would be more useful than other Stellite alloys in severe corrosive environments. The properties of Stellite21 surface coating can be improved by the addition of the embedded hard materials.

5.2 Specimen fabrication and microstructure analysis method

5.2.1 Specimen fabrication

The chemical compositions of Stellite21 powders are given in Table 3-1. It is used to fabricate the hardfacing layer. Direct metal deposition technology is adopted to create the hardfacing layers. In order to minimize the thermal stress, thermal stress control layer is deposited firstly on the substrate, then a Stellite21 coating is deposited on the thermal stress control layer. Afterwards, the deposited samples are heat treatment, because residual stress is left in the internal of deposited region during the deposition of the Stellite21 alloy. Thermal stress treatment can eliminate the internal residual stress. Because the surface of deposited layer is too crude, the surface layer and the near surface region will generate large number of defect during the depositon process, so the surface of the tool must polished to remove the defect concentration area. Figure 5-1 shows the deposition process of the tool. The designed tool is used to produce axles. After forging 10,000 times, the Stellite21 layer of the specimen is investigated. In addition, a new Stellite21 layer is also fabricated using the same deposition process and studied for comparison.

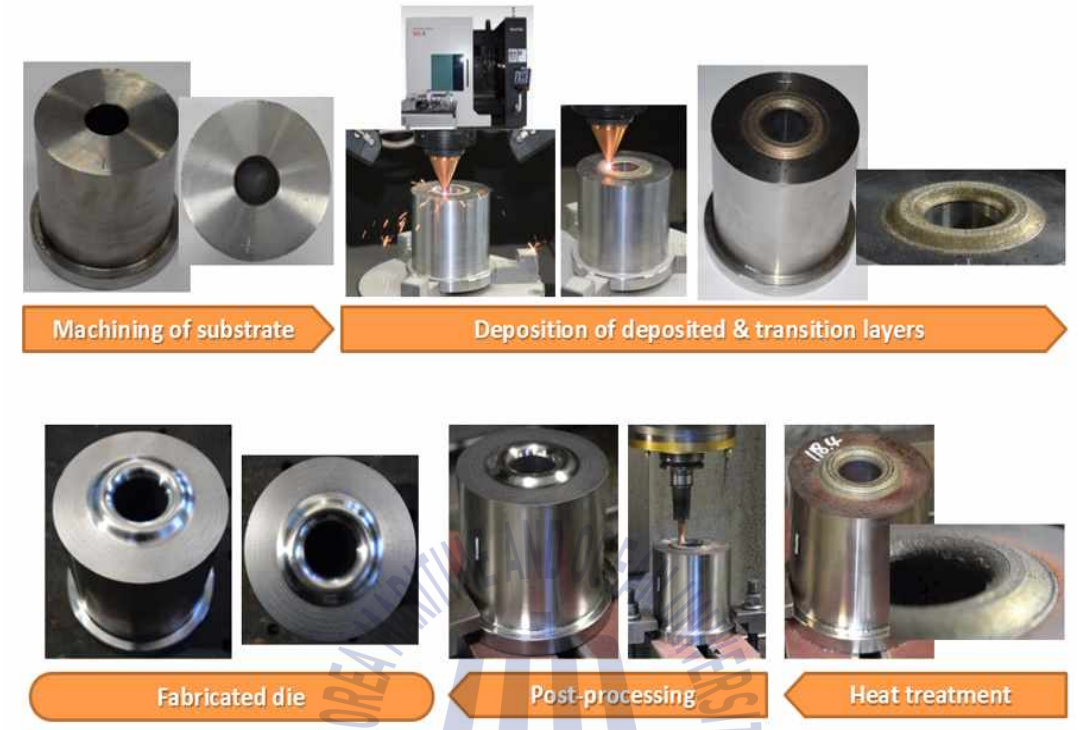

Fig. 5-1 Deposition process of hot forging die

5.2.2 Microstructure analysis method

The top layer of specimen is studied. The harden layer is cut down from specimen, the cutting part is inlaid and polished. The specimen surfaces are ground with papers of 600 to 1500 grit and polished with abrasive cloth plus 1 mm alumina powder. Figure 5-2 shows the polished specimen, the left side is cut from the die after 10000 shots, the right side is the only deposited sample. Two samples are prepared for each type of specimen, one for hardness testing and the other for microstructure observation. The surface corrosion solution of the sample is the solution mixture of 15 mL HNO_3, 15 mL acetic acid, 60 mL HCl, and 15 mL H_2O. The hardness of samples are tested by the microhardness tester. The etched samples are observed under the optical microscope. The microstructure analyses of the specimens are

carried out on a TESCAN MIRA3 scanning electron microscope (SEM) with energy dispersive X-ray (EDX) spectrum. The phases present in the specimens are examined with an X-ray technique, using Cu K_radiation.

(a) specimen after productions of 10000 parts

(b) only deposition specimen

Fig. 5-2 Polished specimen

5.3 Test results and discussion

5.3.1 Comparison of experimental results

In the forging process, hot forging die generally need to experience the effects of high temperature and high pressure, which is a huge test for the abrasive tools. Figure 5-3 shows the wear of a conventional abrasive tool. Figure 5-3 (a) shows the wear after 5,000 operations. It is seen from the figure that most of the convex part of die has been worn off, and the convex top has been flattened. Figure 5-3 (b) shows the abrasive wear after working 10,000 times, it can be seen from the figure that the convex part is almost flat and the abrasive tool is completely scrapped. According to the

actual wear condition of the abrasive tool, it is completely consistent with the simulation of the 3D-DEFORM software. The largest part of the wear is in the convex part, and the flat part of the upper surface has little wear. Therefore, we only hardened the raised part. Figure 5-4 shows the surface wear condition of designed die, this abrasive tool has been forged 10000 times. From the figure, it is seen that the hardened convex portion hardly shows wear and can maintain its original shape. However, after many times of high temperature and high pressure, the internal microstructure of the hardened layer material and its performance will inevitably change.

(a) after production of 5000 parts (b) after production of 10000 parts

Fig. 5-3 Surface wear of conventional die

Fig. 5-4 Surface wear of designed die after production of 10000 parts

In order to make the wear condition of the abrasive tool more specific, the contour of the hot forged abrasive tool after service is drawn. Figure 5-5 shows a comparison of the contours of the hot forging die. The outermost black line is the outline of the designed abrasive tool after forging 10,000 times. The outline of the tool is almost the same as the original contour line. A part of a surface that is connected to a convex part has a certain a mount of wear. The orange outline is the result of a conventional abrasive tool working 5,000 times. The top of the abrasive tool has some wear on the top, and the top is flat. There is almost no wear in the place where surface that is connected to a convex part. The blue outline is the result of 10,000 cycles of the conventional abrasive tool. The raised part is almost flat, and there is

also greater wear in the area where surface that is connected to a convex part.

Figure 5-6 shows the influence of the forged times on the depth of groove of the designed and traditional die[14]. The red line is represented the evaluation line of the wear depth of traditional abrasives with the change of the forging times. From the figure, the wear depth can be increased with the forging time. The wear depth grows exponentially, which is mainly due to the fact that as the number of forgings increases, top surface of the raised part is ground into a plane, the pressure will increase, the mechanical heat and the friction coefficient will also increase, in addition, the strength of die will decrease with temperature increasing. Therefore, abrasive wear will become faster and faster based on the Archard equation. The blue line is represented the evaluation line of the wear depth of designed abrasives with the change of the forging times. It can be seen that wear rate of the die increases linearly, it is more slowly than the traditional abrasive. This is mainly due to the hardness of Stellite21 can keep a high hardness at elevated temperature and the reduced friction coefficient. According to the precise manufacturing requirements of the axle, the wear depth of the abrasive tool cannot be allowed more than 0.5 mm. The conventional die can only use about 3180 times according to requirements, however the designed die can have a service life of about 22,850 times. Therefore, the use of a designed die can greatly extend the life of the abrasive tool.

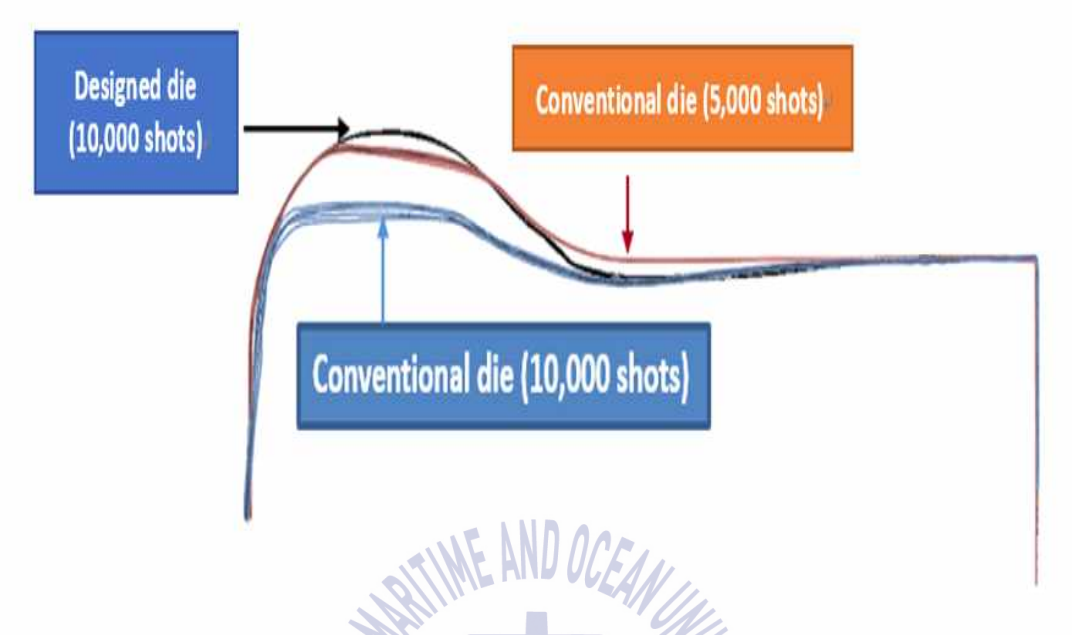

Fig. 5-5 Comparison of contour of hot forging die[14]

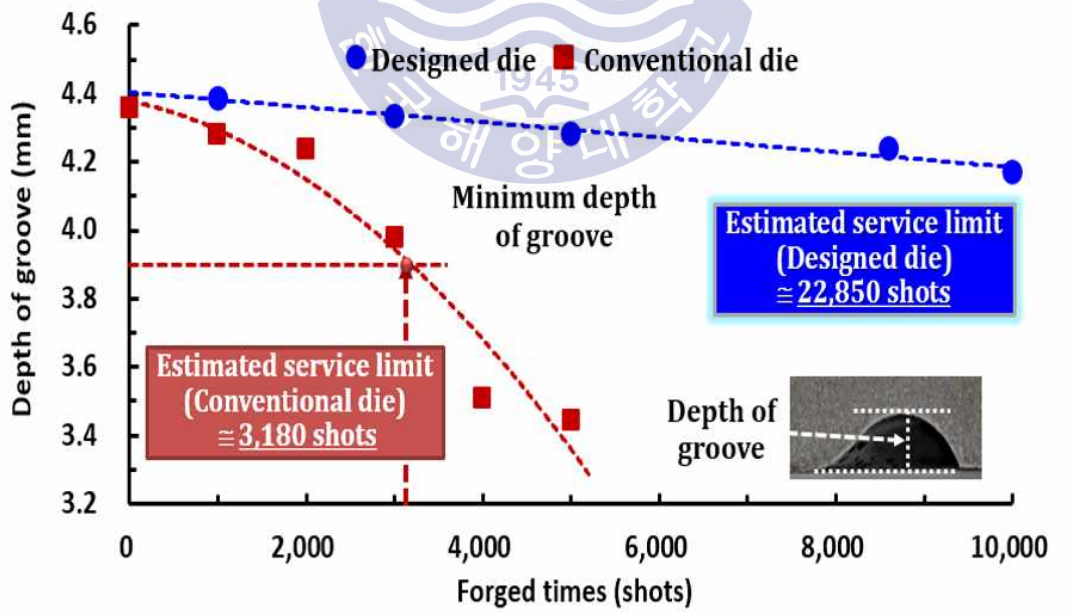

Fig. 5-6 Influence of the forged times on the depth of groove[14]

5.3.2 Fatigue crack analysis

Hot forging die during service has to experience multiple temperature cycles, stress cycles and mechanical friction, the surface of die is prone to fatigue cracks. Figure 5-7 shows the macroscopic morphology of the cross-section of the specimen after 10000 forgings. It can be seen from the figure that there are many cracks on the surface of specimen. The cracks should be formed by both mechanical stress and thermal stress, and all of the cracks almost appear on the top and right side of the convex part. This shows that the top and the right side of the specimen experienced higher thermal stress and mechanical stress.

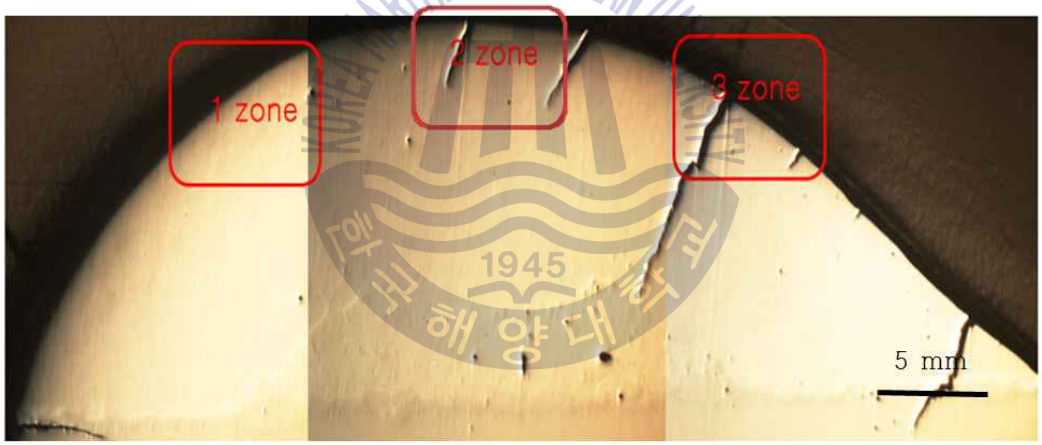

Fig. 5-7 Macro-morphology of the sample section

In order to better understand the cause of crack formation, forging process of axle shaft is simulated by 2D-DEFORM software. According to simulation results, it is investigated the specific conditions of forging die in the forging process, as well as the causes of cracks in the region 2 and 3 and no cracks in the region 1. Figure 5-8 shows the distribution of the surface temperature and the principal strain of the forging die during the forging process. It can be seen that the maximum principal strain and the maximum temperature

occur simultaneously at the top right of the hot forging tool. The highest temperature is found in the area 3, followed by the area 2 place, and area 1 is relatively minimal. The higher the temperature, the lower the hardness of the material, the greater the deformation occurs under the mechanical loading.

Figure 5-9 shows the change of temperature with time during the forging process. After three points of measurement, it is found that the temperature change at point 3 is the fastest, point 2 follows, and point 1 is the smallest. Therefore, there are a large number of cracks in areas 2 and 3, since the highest temperature and the fastest change occur here, it causes the fatigue of the material, resulting in thermal fatigue cracks.

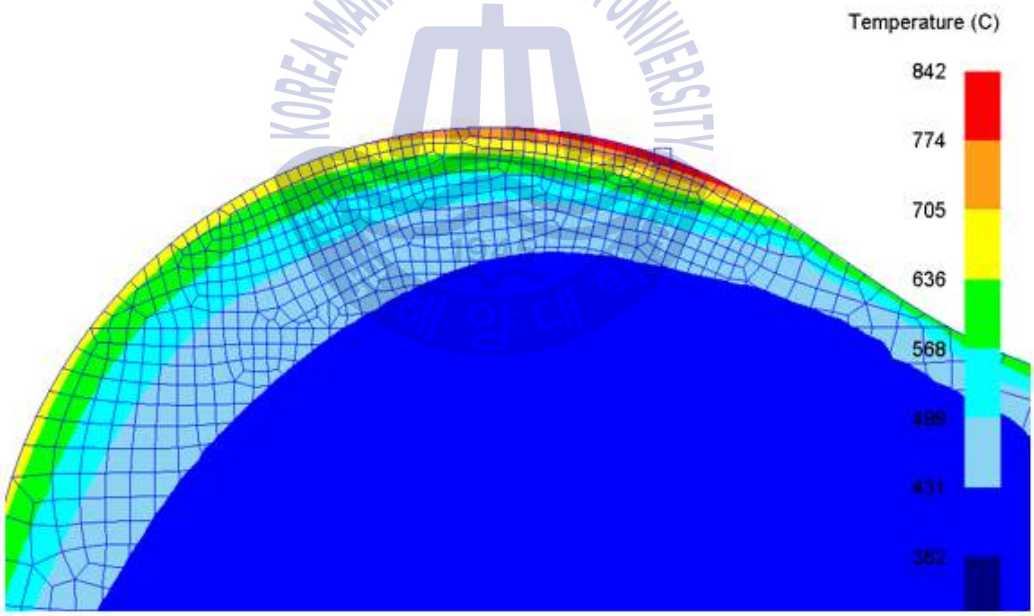

(a) Maximum temperature distribution

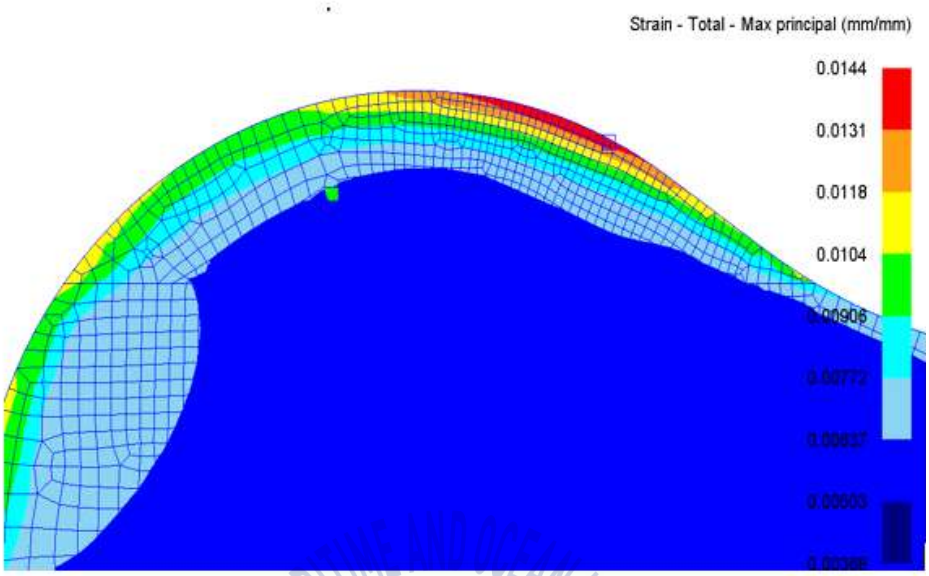

(b) Maximum principal strain distribution

Fig. 5-8 Simulation results of hot forging die

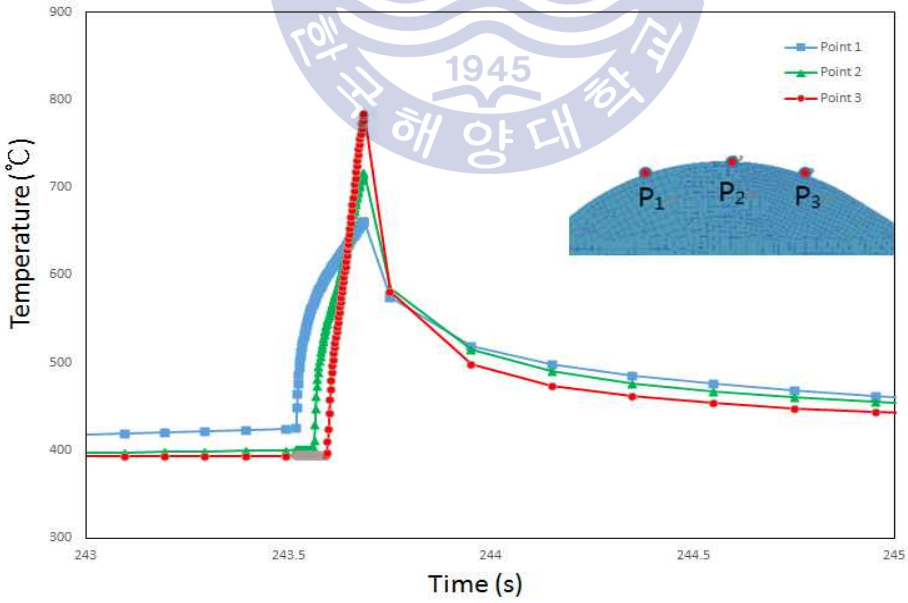

Fig. 5-9 Three-point time-temperature curve on the surface of die

Figure 5-10 shows the microstructure of the three regions at the top of the hardened layer (the three regions are shown in Figure 5-7). It can be seen from the figure that a large number of black microstructures are formed on the grain boundaries. These black structures should be the precipitated carbide, a small amount of carbon atoms and alloy atoms (Cr, Mo, etc.) in the Stellite21 superalloy can form carbide during the forging process. When these hard and brittle carbides are joined together, fatigue cracks are easily generated under the dual effects of mechanical stress and thermal stress. It is seen that the distribution of black carbides are relatively disordered and there is almost no large black line (see Fig. 5-10(a)). From Figures 5-10(b) and (c), it can be seen that the surface of the Stellite21 has a lot of black lines, especially the picture c, which will form early cracks. This is also the reason why a large number of cracks are formed in the regions 2 and 3 in Figure 5-7.

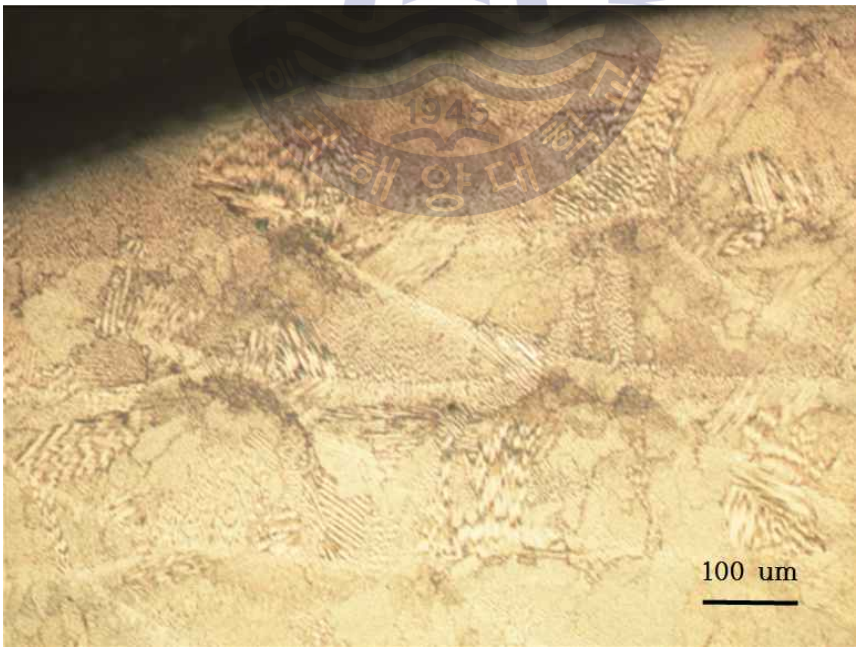

(a) Microstructure of zone 1

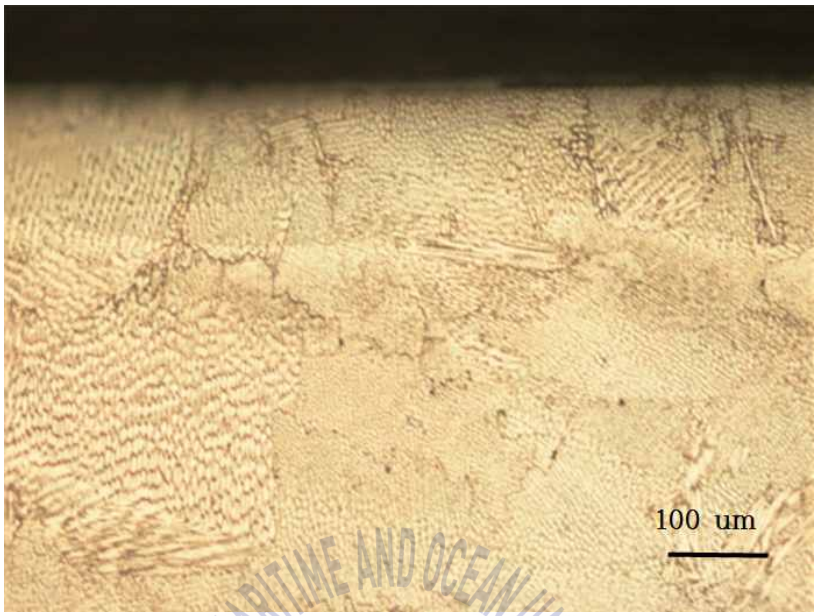

(b) Microstructure of zone 2

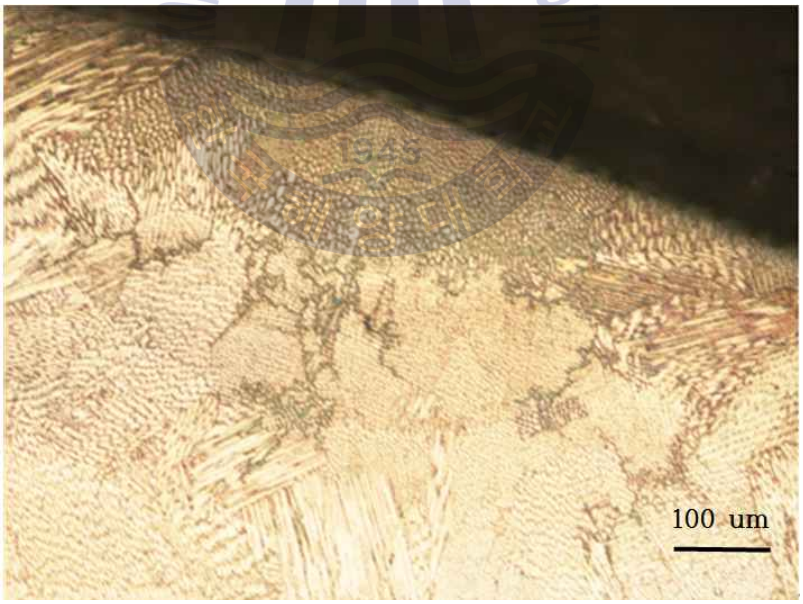

(c) Microstructure of zone 3

Fig. 5-10 Surface microstructure of die

5.3.3 Evolution of hardness of Stellite21 before and after service

Hot forging die will undergo a series of complicated changes during the forging process. The die will be subjected to compressive stress, thermal stress, corrosion and oxidation, and the microstructure and properties of the die materials will change after service. Figure 5-11 shows Comparison of microhardness of specimens before and after service. From this figure, the hardness of Stellite21 after service is greater than that before service, especially on the surface of the hot forging die. After the service, the surface hardness reaches 580 HV, while it is only 440 HV before service. This shows that the microstructure of the Stellite21 has changed during the forging process, resulting in increased hardness.

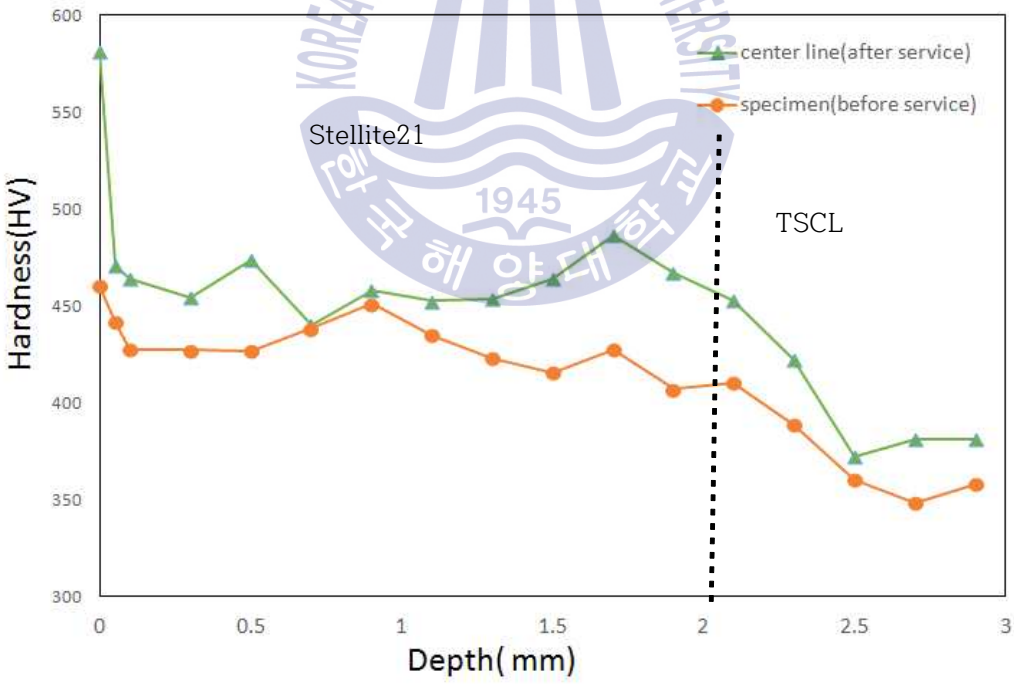

Fig. 5-11 Comparison of microhardness of specimens before and after service

5.3.4 Evolution of microstructure of Stellite21 after service

Figure 5-12 shows scanning electron microscope microstructure of Stellite21 before service. Two types of microstructure can be seen in the figure, one is a white carbide structure that is interconnected into a network, and the other is a gray-black cobalt-based solid solution structure that is filled in a white network. This is because carbide formed in welding process can not dissolves in cobalt-based solid solution, during Stellite21 stacked material natural solidification, carbides are ejected to the grain boundary, these carbides are uniformly and continuously distributed.

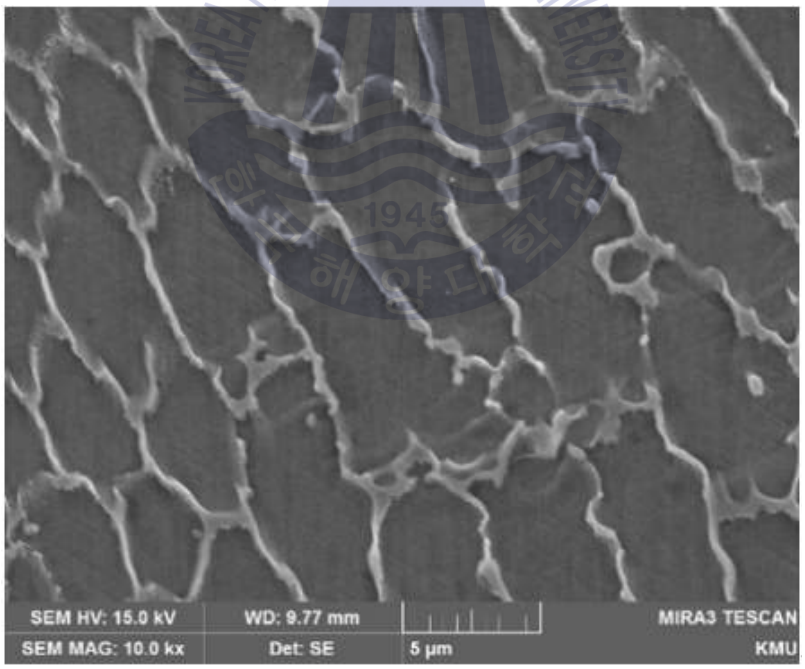

Fig. 5-12 Scanning electron microscope microstructure of Stellite21 before service

Figure 5-13 shows scanning electron microscope microstructure of Stellite21 after service. Figure 5-13 (a) shows microstructure of surface layer of Stellite21. Figure 5-13 (b) shows microstructure of internal layer of Stellite21. It is shown that the amount of white carbide increases obviously in Stellite21 alloy after forging, and the continuous network is broken partially. This is because the temperature of forging die increases during the forging process. The inside of hardened layer material Stellite21 will have a carbide precipitated. The formation of carbides causes the increase of hardness, and at the same time, the temperature of die rapidly decreases after the forging process. This may lead to the aggregation of carbides, so that there is a discontinuity in the continuous network structure. Comparison of Figure 5-13(a) and (b), it is seen that the surface of the Stellite21 forms more white carbides than internal, and the distribution of carbides is more focused. So that the surface hardness increase, but toughness decrease. It may be leads to form fatigue cracks during hot forging process. Comparison of Figure 5-12 and 5-13, it is shown that carbide formation in Stellite21 after service is much more than that before service, so the hardness of Stellite21 after service is higher than that before service.

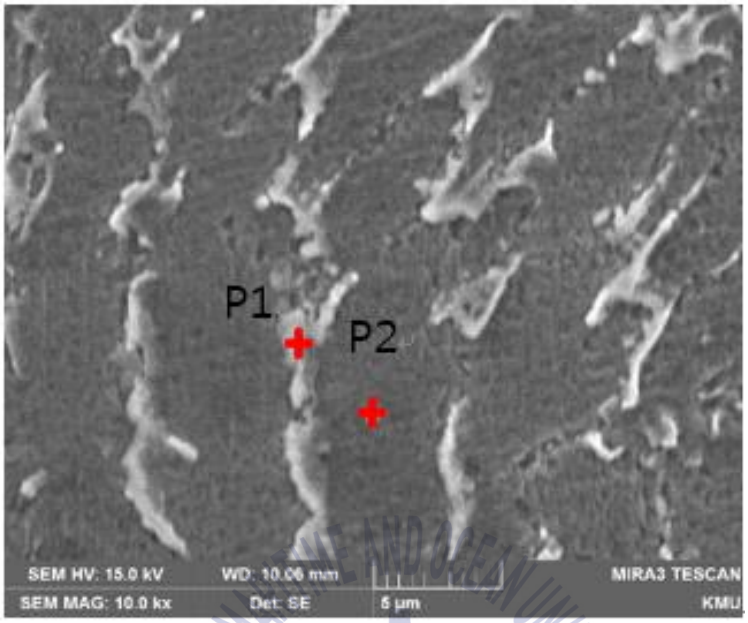

(a) Microstructure of surface layer of Stellite21

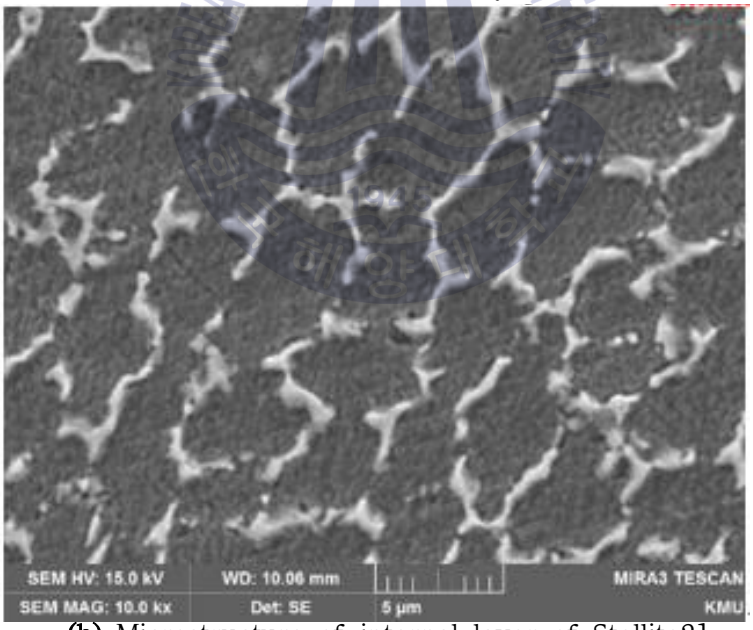

(b) Microstructure of internal layer of Stellite21

Fig. 5-13 Scanning electron microscope microstructure of Stellite21 after service

Figure 5-14 shows the chemical composition and energy spectrum of the special tissue in the Stellite21 hardened layer produced by laser cladding. From the figure 5-14(a), the white line microstructure (point 1 in Figure 5-13(a)) contains more carbon, chromium, molybdenum and cobalt. This is an often formed $M_{23}C$ compound in the Stellite21 alloy. This carbide formation can increase the hardness of the Stellite21, so when the Stellite21 undergoes forging service, a large amount of $M_{23}C$ compound is internally produced, making the Stellite21 harder, especially the surface[58]. The black microstructure (point 2 in Figure 5-13(a)) in the figure 5-14(b) contains a large amount of cobalt and chromium, so this material is a cobalt-based solid solution.

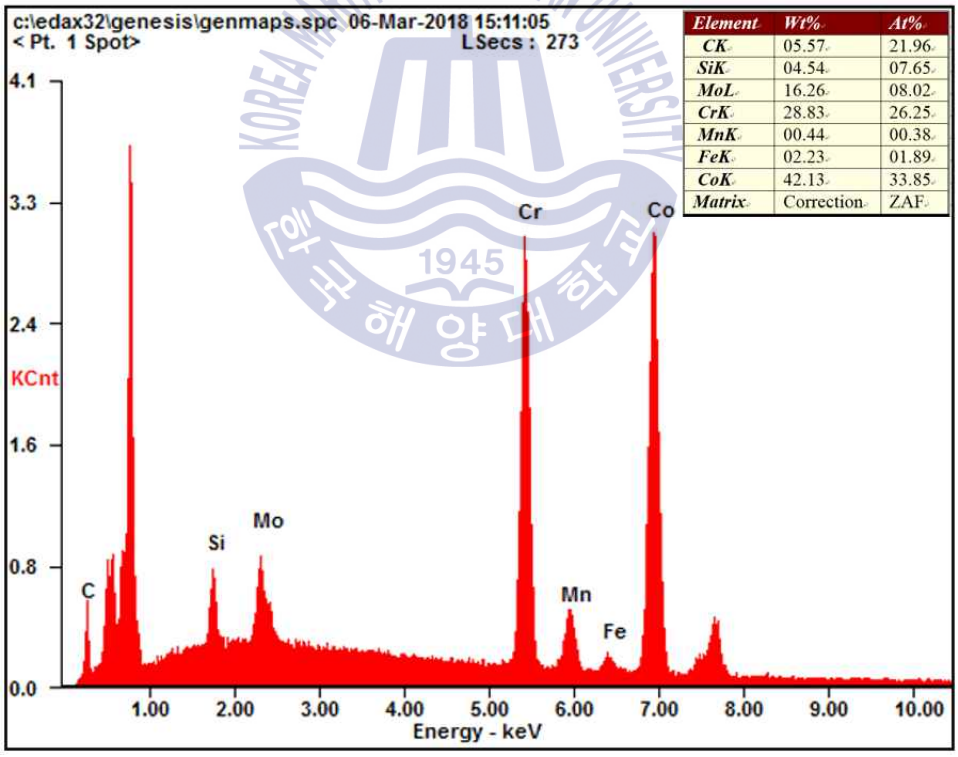

(a) Point 1

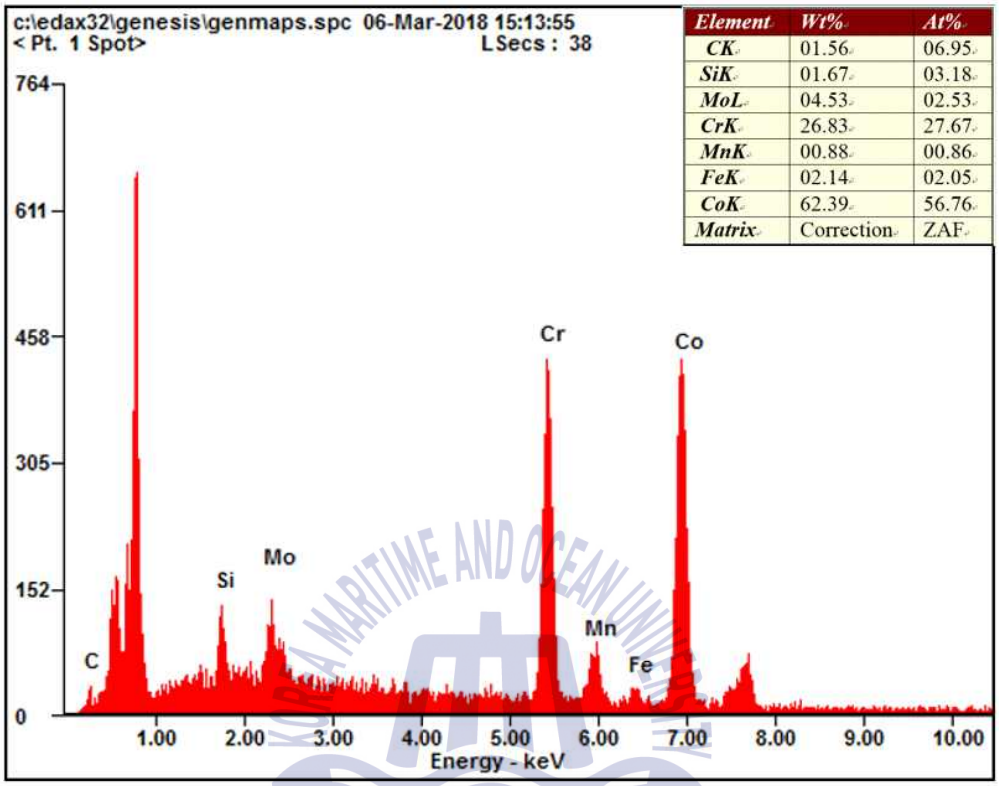

(b) Point 2

Fig. 5-14 Chemical composition of special spots and their energy spectrum diagram

XRD patterns of Stellite21 before and after service have been shown in Figure 5-15. This figure shows that Stellite21 before service includes γ-Co (fcc) phase with <001> and ε-Co (hcp) phase with <0001>; however, Stellite21 after service on only includes γ-Co (fcc) phase with <001> and ε-Co (hcp) phase with <0001>, but also includes ε-Co (hcp) phase with <1011>. According to the peak value, the forged Stellite21 contains more ε-Co (hcp) phases. Since the ε-Co (hcp) phase does not increase the

hardness of the Stellite21, it can also reduce its friction coefficient, so the Stellite21 can have a better wear resistance[59-61].

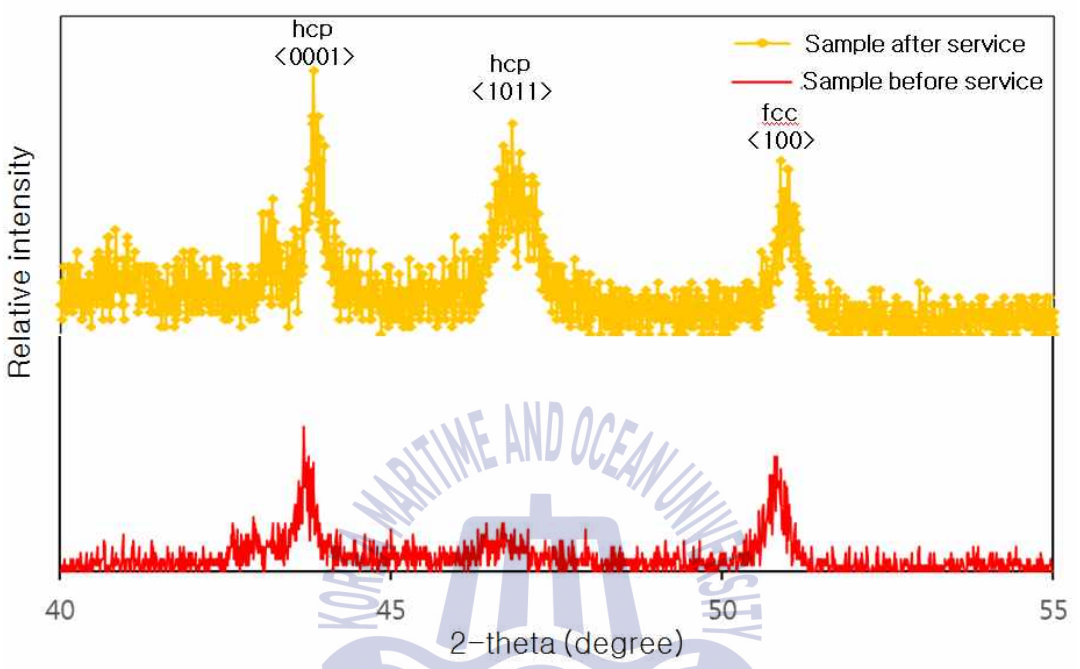

Fig. 5-15 XRD patterns of Stellite21 before and after service

Chapter 6 Conclusion

In this study, the surface hardening of hot forging die for automobile axles is researched, and the service life of hot forging die is extended by increasing the surface strength and wear resistance. The finite element method is used to predict the wear part of hot forging die and the hardened layer to be designed. Also the thermal stress between the hardness layer and the base layer are studied. To control thermal stress between the deposited region and the base metal for hot forging of axle, the TSCL is designed and analyzed sing numerical analysis methods. The numerical simulation results demonstrate that the thermal stress between the deposited region and the base metal is effectively controlled by changing the TSCL thickness and mixing ratio. Finally, Stellite21 alloy is studied. The microstructure and properties are investigated before and after forging. The following are conclusions :

(1) 3D-deform software is used to analyze the interfacial stress, interface temperature and slip speed of the abrasive tool, the maximum wear depth and position of the abrasive tool is simulated, and the hardened layer according to the simulation results is designed.

(2) TSCL thickness and composition have different effects on the size of thermal stress. When the thickness of the TSCL is increased and the composition of the TSCL is constant, the deviation of maximum principal stress is decreased. However, when the thickness of the TSCL reaches 2 mm, the deviation of principal strain is very high. When the Stellite21 volume ratio of the TSCL is increased while maintaining the thickness of the TSCL, the deviation of principal stress is decreased on the interface between the hardfacing layer and TSCL; but it is increased on the interface between the TSCL and the substructure.

(3) Taking into account the deviation of maximum principal stress and strain at the interface of the TSCL, a TSCL with thickness of 1.5 mm and the 50% Stellite21 mixing ratio is the optimal design of deposition using the 3D printing technique.

(4) The hardened layer will experience fatigue cracking when it undergoes multiple thermal cycling and mechanical stresses. The formation of fatigue crack cracks is caused by both internal and external causes of the material. Continuous carbides are produced inside the material to provide conditions for the formation of cracks, and the outside of the material is subjected to continuous effects of thermal stress and mechanical stress.

(5) The hardness of Stellite21 increases after service, especially on the surface of the material. This is mainly due to the formation of a large amount of carbides inside the material after service, which increases the hardness of the material, and a large amount of γ-cobalt transforms into ε-Co solid solution under the action of strain.

Outlook

After Stellite21 is used to strengthen the surface of the forging die of the automobile axle, its service life has been significantly improved. However, the process requires high precision, relatively complicated, and high cost. Secondly, the surface of the uncured abrasive tool is still worn near the hardened zone. Thirds, the fatigue cracks occurs on the surface of the Stellite21 after hot forging. In view of the above questions, our next goal is to study these issues. The specific method is as follows: (1) Improve manufacturing processes, such as improve deposition efficiency while ensuring quality, etc; (2) Adjust deposition region and TSCL to reduce wear and thermal stress; (3) Using the new modified Stellite21 as harden materials, for example, add a small amount of rare element Yttrium into Stellite21 to enhance the wear resistance of Stellite21.

Acknowledgements

After three months of hard work, I finally completed the work of the thesis. First of all, I would like to thank my advisor and Professor, Dr. Jong-Rea Cho, for his great help during the entire period of my doctor' research and writing of the thesis. Whenever I have problems that are difficult to solve, he can always give me a new idea and solutions using his profound knowledge and the rich experience. Here, I would like to express my deep gratitude and respect to Professor Jong-Rea Cho once again. Secondly, I would like to thank my teachers and labmates who have directly and indirectly helped me during these three years, and thank you for your help in life and study. Finally, I would like to thank my parents and my wife, thank you for your support, encouragement and companionship.

References

1. Lange, K., Cser, L., Geiger, M., and Kals, J. A. G., "Tool Life and Tool Quality in Bulk Metal Forming," Annals of CIRP, Vol. 41, No. 2, pp. 667-675, 1992.
2. L. Cser, M. Geiger, K. Lange, "Tool life and tool quality in bulk metal forming", Proc. Inst. Mech. Engrs. Vol. 207 pp. 223-239, 1993.
3. Gong Hongliang, Mechanism and Method of Relieving Thermal Stress in Hot Forging Die. Wuhan university of technology. 2007.
4. Kang, J.H., Park, I.W., Jae, J.S., and Kang, S.S., "A Study on a Die Wear Model Considering Thermal Softening: (I) Construction of the Wear Model," J. Mater. Process. Technol., Vol. 96, No. 1-3, pp. 53-58, 1999.
5. Kang, J.H., Park, I.W., Jae, J.S., and Kang, S.S., "A Study on a Die Wear Model Considering Thermal Softening: (II) Application of the Suggested Wear Model," J. Mater. Process. Technol., Vol. 94, No. 2-3, pp.183-188, 1999.
6. Doege, E., Groche, P., and Bobke, T., "Application of Adhesion Theory to Friction and Wear Processes in Hot Die Forging," Advanced Technology of Plasticity, Vol. 1, pp. 27-32, 1990.
7. De Oliveira, U., Ocelik, V., De Hosson, J.T.M., "Analysis of Coaxial Laser Cladding Processing Conditions," Surf. Coatings Technol., Vol. 197, No. 2, pp. 127-136, 2005.
8. Wu, X. and Chen, G., "Microstructure and Wear Resistance of In situ TiCp Composite Coating by Laser Cladding," J. Mater. Sci. Technol., Vol.15, No. 3, pp. 233-238, 1999.
9. Moures, F., Cicalã, E., Sallamand, P., Grevey, D., Vannes, B., Ignat, S., "Optimisation of Refractory Coatings Realised with Cored Wire Addition Using a High-power Diode Laser," Surf. Coatings Technol., Vol. 200, No. 7, pp. 2283-2292, 2005.
10. Park, N.-R. and Ahn, D.-G., "Wear Characteristics of Stellite6 and NOREM02 Hardfaced SKD61 Hot Working Tool Steel at the Elevated Temperature," Int. J. Precis. Eng. Manuf., Vol. 15, No. 12, pp. 2549-2558, 2014.
11. Köhler, H., Partes, K., Kornmeier, J.R., Vollertsen, F., "Residual Stresses in Steel Specimens Induced by Laser Cladding and Their Effect on Fatigue Strength," Physics Procedia, Vol. 39, pp. 354-361, 2012.

12. Ocylok, S., Weisheit, A. and Kelbassa, I., “Functionally Graded Multi-layers by Laser Cladding for Increased Wear and Corrosion Protection,” Physics Procedia, Vol. 5, Part A, pp. 359-367, 2010.
13. Park N.R., Ahn, D.G., and Oh, J.W., “Estimation of the Thickness and the Material Combination of the Thermal Stress Control Layer (TSCL) of the Stellite21Hardfaced STD61 Hot Working Tool Steel Using Three-Dimensional Finite element Analysis,” Trans. Korean Soc. Mech. Eng. A, Vol. 38, No. 8, pp. 857-862, 2014.
14. Ahn, D. G, Lee, H. J., Cho, J. R., Guk, D. -S., “Improvement of the wear resistance of hot forging dies using a locally selective deposition technology with transition layers,”CIRP Annals-Manufacturing Technol., Vol.65, No.1, pp.257-260, 2016.
15. Tang liuding. Shi yuhuan. Meng Jin. Analysis of fatigue life of hot dies with small surface cracks. Journal of Henan University of Science and Technology (Natural Science Edition). Vol. 5(26): 8-11, 2005.
16. Jiang Xiuzhi, Stress and damage styles of the hot forging die. Die and Mould technology, Vol. 2: 39-50, 1993.
17. Falk B, Engle U. Etc. Estimation of tool life in bulk metal forming based on different failure concepts. Journal of Materials Processing Technology, Vol. 80-81: 602-607, 1998.
18. Lin Huiguo. Mold material application manual, version 2[M]. Beijing: Machinery Industry Publishing, Vol.8: 276-282, 1983.
19. Suresh S, Material fatigue, version 2[M]. Beijing: National Defense Industry Publishing, pp. 385-388, 1999.
20. Cai Huaicong, Min Xing, Material mechanics [M], Xi’an Jiaotong University Publishing, Vol.1: 266-274, 2004.
21. A. B. Lei Kefu. Heat conduction theory [M]. Beijing: Higher Education Publishing, Vol.12, 1959.
22. S. L. Semiatin et. a1., Determination of the Interface Heat Transfer Coefficient for Nor-Isothermal Bulk-Forming Processing[J] . Transactions of the ASME , Journal of Engineering for Industry, Vol.109 : 49-57,1987.
23. Liou, M., and Hsiao, H., “Prediction of Die Wear in High Speed Hot Upset Forging,” Report No. ERC/NSM-88-33, Engineering Research Center for Net Shape Manufacturing, Oct 1988.
24. T. Altan, G. Ngaile and G. Shen, “Cold and Hot Forging-Fundamentals and

Applications", March 2004.
25. "Metals Handbook - Forging and Casting", Vol. 5, 8th Edition, ASM Handbook Committee, USA, 1971.
26. Hayashi, C., Shinoda, T. and Kato, Y., Bead Shape on Directed Plasma Fabrication Process, Journal of the Society of Materials Science, Japan, Vol.51(9): 1045-1050, 2002.
27. Daiss, S., Bischoff, E. and Gruenenwald, B.. Metallographic Characterization of Stellite/WC Composite Layers Produced by Laser Cladding, Practical Metallography, Vol.33(2): 99-111, 1996.
28. Persson, D. H. E., Jacobson, S. and Hogmark, S. . The Influence of Phase Transformations and Oxidation on the Galling Resistance and Low Friction Behavior of a Laser Processed Co-based Alloy, Wear, Vol. 254(11-12): 1134 -1140, 2003.
29. Persson, D.H.E., Jacobson, S. and Hogmark, S.. Effect of Temperature on Friction and Galling of Laser Processed Norem 02 and Stellite21, Wear, Vol. 255(1-6): 498-503, 2003.
30. Kang, S.H., Shinoda, T., Kato, T. and Jeong, H.S.. Thermal Fatigue Characteristics of PTA Hardfaced Steels, Surface Engineering, Vol. 17(6): 498-504, 2001.
31. Tuominen, J., Hayhurst, P., Eronen, V., Vuoristo, P. and Mantyla, T.. Comparison of Multi-feed and Off-axis High Power Diode Laser (HPDL) Cladding, In: Proceedings of SPIE - The International Society for Optical Engineering, Vol. 4973, pp. 116-127, 2003.
32. Chan, W.S., Lui, T.S. and Chen, L.H.. Solidification Structure of Stellite Overlayer Formed on Spheroidal Graphite Cast Iron by Plasma Transferred Arc Process, Materials Transactions, JIM, Vol.35(8): 529-537, 1994.
33. Disam, J., Luebbers, K. and Sickinger, A.. In: Proceedings of the National Thermal Spray Conference, Thermal Spray Coatings: Properties, Processes and Applications, Orlando, Florida, USA, pp. 229-235,1992 .
34. Han, D. and Mecholsky, J.J. Jr.. Fracture Behavior of Metal Particulatere-inforced WC-Co Composites, Materials Science and Engineering A, 144(1-2): 293-302, 1991.
35. Lee. J. H, Kim. D. J, Kim. B. M and Kim. H. K,, "Wear Analysis of Hot Forging Die Consider Thermal softening", Transaction of Materials Processing, Vol. 9, No. 1, 2000.

36. Achard. J. F,, “Contact and rubbing of flat surfaces”, Journal of applied physics, pp. 981-988, 1953.
37. Taylan Altan, “Cold and Hot Forging Fundamentals and Applications”,The materials Information society.
38. Lee. R. S, Jou. J. L,, “Application of numerical simulation for wear analysis of warn forging die”, Journal of Material Processing Technology, Vol.140, pp.43-48, 2003.
39. Farren, W.S., Taylor, G.I.,”The Heat Developed During Plastic Extrusion of Meatals,” Proc. R. Soc., Ser. A, vol. 107, pp. 422-451, 1925,.
40. Ahn, D. G., “Application of Laser Assisted Metal Rapid Tooling Process to Manufacture of Molding & Forming Tools-State of the Art,” Int. J. Precis. Eng. Manuf., Vol. 12, No. 5, pp. 925-938, 2011.
41. Jiang, W, and Molian, P., “Laser Based Flexible Fabrication of Functionally Graded Mould Inserts,” Int. J. Adv. Manuf. Technol., Vol. 19. No. 9, pp. 646-654, 2002.
42. Jianli, S., Yongtang, L., Qilin, D., and Dejin, H., “Experimental Study of Laser Cladding Forming Iron-based Alloy,” Proc. of Technology and Innovation Conference, pp. 1463-1467, 2006.
43. Khalid Imran, M., Masood, S. H., Brandt, M., Bhattacharya, S., and Mazumber, J., “Direct Metal Deposition(DMD) of H13 Tool Steel on Copper Alloy Substrate: Evaluation of Mechanical Properties,” Mater. Sci. Eng. A, Vol.528, No. 9, pp.3342-3349, 2011.
44. Suh, J. H., Kim, J. S., Han, J. H., Lee, D. H., and Hwang, S. S., “Development of a Technology for Amorphous Material (Co-free) Hardfacing on Primary Side Component Materials Using Laser Beam to Improve Their Wear, Erosion, Corrosion Resistance,” KAERI, 2000.
45. Kaiele, S., Barroi, A., Noelke, C., Hermsdorf, J., Overmeyer, L., and Haferkamp, H., “Review on Laser Deposition Welding: From Micro to Macro,” Physics Procedia, Vol. 39, pp. 336-345, 2012.
46. Thivillon, L., Bertrand, P., Laget, B., and Smurov, I., “Potential of Direct Metal Deposition Technology for Manufacturing Thick Functionally Graded Coatings and Parts for Reactors Components,” J. Nuel. Mater., Vol. 385, No. 2, pp. 236-241, 2009.
47. Majumdar, J. D., “Laser Assisted Composite Surfacing of Materials for Improve Wear Resistance,” Physics Procedia, Vol. 5, Part A, pp.425-430,

2010.
48. Paul, C. P., Mishra, S. K., Premsingh, C. H., Bhargava, P., Tiwari, P., and Kukreja, L. M., "Studies on Laser Rapid Manufacturing of Cross-thin-walled Porous Structures of Inconel 625," Int. J. Adv. Manuf. Technol., Vol. 61, No. 5-8, pp. 757-770, 2012.
49. De Hosson, J.T.M. and de Mol Van Otterloo, L., Surface engineering with lasers: Application to Co based materials, Surface Engineering, Vol.13(6), p. 471-481, 1997.
50. Liu, C.A., Humphries, M.J. and Mason, D.W., Effectt of laser-processing parameters on the formation and properties of a Stellite hardfacing coating, Thin Solid Films, Vol. 107(3), p. 251-257, 1983.
51. Kathuria, Y.P. and Tsuboi, A., Laser cladding of Stellite #6: A detailed analysis, Proceedings of the SPIE The International Society for Optical Engineering, Vol. 2789, pp.86-92, 1996.
52. Frenk, A., Henchoz, N. and Kurz, W., Laser cladding of a cobalt-based alloy: Processing parameters and microstructure, Zeitschrift fuer Metallkunde, Vol. 84(12), p. 886-892, 1993.
53. Colaco, R., Carvalho, T. and Vilar, R., Laser cladding of Stellite 6 on steel substrates, High Temp. Chem. Processes, Vol.3, pp. 21-29, 1994.
54. Frenk, A., et al., Analysis of the laser-cladding process for stellite on steel, Metallurgical and Materials Transactions B: Process Metallurgy and Materials Processing Science, 28(3), p.501-508, 1997.
55. Jeong, J.S. and Shin, K.H, "Fabrication of Functionally Graded Materials between P21 Tool Steel and Cu by Using Laser-Aided Layered Manufacturing," Trans. Korean Soc. Mech. Eng. A, Vol. 37, No. 1, pp. 61-66, 2013.
56. Jang, S.P. and Choi, S.U.S., "Effects of Various Parameters on Nanofluid Thermal Conductivity," Trans. AMSE J. Heat Transfer, Vol. 129, No. 5, pp. 617-623, 2006.
57. Davis, J.R. Properties and Fabrication Characteristics of Cobalt and Cobalt Alloys, In: Nickel, Cobalt, and Their Alloys, Materials Park, USA. pp. 371-401, 2000.
58. Sh. Zangeneh, H.R. Lashgari, H.F. Lopez, H.K. Farahani, Microstructural characterization of TIG surface treating in Co-Cr-Mo-C alloy, Materials Characterization, Vol. 132, pp 223-229, 2017.

59. Ad Saldivar Garxcia, A.M. Medrano, A.S. Rodriguez, Formation of hcp martensite during the isothermal aging of an fcc Co-27Cr-5Mo-0.05C orthopedic implant alloy, Metal. Mater. Trans. Vol. 30(5) 1177-1184, 1999.
60. H.F. Lopez., A.J. Saldivar-Garcia, Matensitic transformation in a cast Co-Cr-Mo-C alloy, Metal. Mater. Trans. Vol. 39 (1) pp. 8-18, 2008.
61. A.J. Saldivar-Garcia, H.F. Lopez, Temperature effects on th lattice constants and crystal structure of a Co-27Cr-5Mo low-carbon alloy, Metal. Mater. Trans. Vol. 35 (8), pp.2517-2523, 2004.